# Dynamic magneto-flexoelectricity and seismo-electromagnetic phenomena: Connecting mechanical response to electromagnetic signatures

Antonios E. Giannakopoulos [a,*], Ares J. Rosakis [b]

[a] *Mechanics Division, National Technical University of Athens, Greece*
[b] *Graduate Aerospace Laboratory, California Institute of Technology, Pasadena, CA 91125, USA*

ARTICLE INFO

ABSTRACT

The electromagnetic aspects of the fully dynamic flexoelectric problem are examined for dielectric solids by introducing a new theoretical framework which incorporates both gradients of electric polarization and flexoelectricity due to strain gradients and also includes a weak coupling with the magnetic field. This formulation predicts the existence of linear relations between the electric field and the dilatational components of the particle accelerations. It also shows that the magnetic flux and the magnetic field are proportional to the shear components of the particle velocities. Our continuum theory, although based on very different assumptions, seems to be analogous to the electrokinetic theory of Pride which has been used to assess seismo-magnetic phenomena and measurements in earthquake events.

## 1. Introduction

Flexoelectricity is the ability of materials to convert mechanical strain gradients to electric polarization and vice versa and exists in all dielectric materials. An excellent recent perspective of this unusual electromechanical coupling with emphasis on applications in energy harvesting, micro-electro-mechanical systems, nanotechnology, and biology can be found in Tripathi el al. (2021) as well as other review articles like (Tagantsev, 1991; Yudin and Tagantsev, 2013; Zubko et al., 2013; Kritchen and Sharma, 2016; Jiang et al., 2013; Wang et al., 2019; Deng et al., 2020) to mention but few. However, an electric field that changes with time gives rise to a magnetic field that has to be accounted for. It is the purpose of this work to investigate the electromagnetic fields ensuing from the flexoelectric theory.

There is ample theoretical work on flexoelectricity in both static and dynamic context, and the most recent ones include the works of Majoub et al. (2008), Hu and Shen (2009), Sharma et al. (2010), Shen and Hu (2010), Hu et al. (2018). There are numerous publications related to examples and applications, several of them can be found in the fore-mentioned review articles. One of the most important classes of applications for which Flexoelectricity theory becomes very useful is related to many dynamical problems encountered in both engineering and in the Geosciences. Indeed, these include many important cases where stress wave- and shock wave-induced loading enhances the flexoelectric response and influences materials behavior and device reliability. The commonality between such applications is the existence of very high strain gradients related to dynamic loading. As only one example, from Engineering, the protection of electronic devises and high-pressure diagnostic equipment from spurious electrical effects, when

---

* Corresponding author.
  *E-mail address:* agiannak@central.ntua.gr (A.E. Giannakopoulos).

mechanically shocked during operation (e.g. impact from accidental drop, explosion etc.), brings about the dramatic drop of electric resistivity of many dielectrics subjected to mechanical shock conditions. Impact-induced strain gradients in such problems are typically very high, therefore the flexoelectric phenomenon could account for such electric resistivity observations.

Similar phenomena, occurring at a vastly different length scale can also be found in the field of Earthquake Source Mechanics. Here dynamic shear ruptures propagating along faults are known to be the key mechanism of generating earthquakes (Aki and Richards, 1980; Ida and Aki, 1972). These ruptures can propagate at various speeds and depending on such speeds; the surrounding rock will be subjected to a high strain gradient field whose nature, at the near field, will also depend on the rupture tip speed.

The recent experimental discovery by Rosakis and his group (Liu et al., 1993; Rosakis et al., 1999; Xia et al., 2004) of super-shear dynamic ruptures, whose speeds exceed the shear wave speed represents an extreme case involving the most severe localization of strain gradients across Mach-Cone structures emanating from the rupture tip and has once again brought to the forefront the suspected connection between shock wave fronts (both shear and/or dilatational) and the flexoelectric response as well as the associated electromagnetic emissions. It has also motivated our most recent work on this subject (Giannakopoulos and Rosakis, 2020). The analogue experiments referred to above, are designed to mimic real earthquake events in the lab scale. They have typically been performed in specimens made of polymers such a PMMA (an isotropic, strongly flexoelectric polymer) and have revealed the existence of Mach-line structures when characteristic speeds are exceeded by the ruptures. Such Mach-like structures, remain almost un-attenuated away from the frictional fault planes (fault), sweeping the solid during rupture growth, and inducing very large strain rates,along the shock length, and very high local strain gradients across it (Rosakis et al., 2020). Regarding large scale, as opposed to laboratory scale Earthquakes ruptures, the experimental discovery of supershear ruptures in the lab has motivated field seismologist to look closer at field evidence for large-magnitude earthquakes propagating at supershear speed and as a result the reporting of such events, formerly thought to be rare, have significantly multiplied (e.g. Bouchon et al., 2001; Ellsworth et al., 2004; Bao et al., 2019; Elbanna et al., 2021; Amlani et al., 2022, just to name a few). Given that supershear rupture is indeed a high possibility during large real earthquakes and that many crustal rock types (much like some of the polymers used in the experiments) are also known to be flexoelectric, the existence of the anticipated Mach-lines at the rupture tips is expected to promote especially strong flexoelectric effects during supershear earthquakes, and are thus of great relevance to the present study as a possible source of very strong electromagnetic emission.

Many of the rock types that comprise the earth's crust and mantle exhibit flexoelectricity, often combined with piezoelectricity (which is only relevant in the case of anisotropy). Electromagnetic emission associated with rock and ice fracture has been recorded (see for example Ogawa and Oike, 1985; Yamada et al., 1989; Fifolt et al., 1993; Yoshida et al., 1998) and has been related to earthquakes, e.g. (Gakhberg and Morgounov, 1982; Draganov et al., 1991). Co-seismic electric and magnetic signals have been recorded in natural earthquakes (Matsushima et al., 2002; Johnston et al., 2006; Honkura et al., 2009; Ujihara et al., 2004; Gugliemi et al., 2006). Several possible models and micro-mechanisms have been proposed to explain the physics involved in producing such emissions. A possible reason for the electromagnetic emission for non-piezoelectric rocks (sandstone, marble, limestone) and ice may be the flexoelectric effect, as suggested by Petrenko (1993) and discussed above.

Yet another mechanism of electromagnetic emission can be found in the work of Bordes et al. (2008) and Garambois and Dietrich (2001) who based their analysis on the theory of Pride (1994). When seismic waves travel in porous materials that contain fluids (mainly water), a relative fluid-grain velocity develops. At the grain-fluid interfaces, a bound surface charge appears and then the electrically balanced free ions in the fluid move, generating an electric streaming current, ensuing electromagnetic phenomenon related to the mechanical deformation. Pride developed a complete macroscopic theory based on the governing equations of poroelasticity (Biot) and of electromagnetism (Maxwell), introducing two coupling equations through an electro kinetic coupling coefficient. The transport equations were formulated through averaging the ion activity in the fluid phase. As a result, the relative fluid-grain velocity can depend on the electric field and the streaming current can depend on the Darcy filtration velocity.

A recent review with many important references on the electrokinetic seismo-magnetics can be found in (Jouniaux and Zyserman, 2016). This work teats a sedimentary rock as a composite of grains and water (or other electrolyte). The solid-fluid interaction follows from the well-known Biot theory. At the solid-fluid interface electric charge is adsorbed by the solid grains, balanced by the ions that flow in the liquid due to the presence of mechanical stresses and as a result, the electric field is established by the electrokinetic mechanism. Their key result is that the electric field developed inside the material is proportional to the acceleration of the mechanical displacement while the magnetic field is proportional to the mechanical velocity. Misutani et al. (1976) indicated that the electrokinetic phenomenon of fissured rocks saturated with water applies to many earthquakes like the Matsuhiro earthquake swarm; see for example (Enomoto et al., 2017). The electrokinetic mechanism may be related to them, as was anticipated early on by Ishido and Mizutani (1981) and Mizutani and Ishido (1976). The amplitudes of such signals range in 1-100 mV/km for the electric field and 0.01-1 nT for the magnetic flux (Ren et al., 2015).

In what we discuss here, flexoelectricity is considered to be the only source of strain gradient effects, and the coupling of the mechanical problem is analogous to a problem of couple stress elasticity where the two characteristic types of lengths emerge as a combination of mechanical, dielectric and flexoelectric constants, as discussed in Giannakopoulos and Rosakis (2020). The first type of length resembles the (well known in the context of couple stress elasticity) microstructural length which is connected to the displacement curvature (see also the anti-plane problem in static form by Gavardinas et al (2018) and in dynamic form by Giannakopoulos and Zisis (2019, 2021)). The second type of length is less referenced (and hardly considered in metrology) and resembles the micro inertial length that essentially introduces a non-classic kinetic energy term that connects to the micro-rotations of the matter. In addition to what was discussed by Giannakopoulos and Rosakis, in our present model we also include additional modeling elements reflecting the important fact that the electric polarization acceleration leads to electromagnetic emission. Including this behavior in our model is in line with experimental evidence in laboratory fractures of ice and rocks and in field measurements prior and during to

earthquake events. Our present work also shows that the electrokinetic model of Pride, developed for dynamic seismo-electromagnetic phenomena in porous media, is very similar to a dynamic flexoelectric model, augmented to include the magnetic field through a weak interaction established by Mindlin and Toupin (1971).

The results of the present work imply that electromagnetic phenomena related to a multiplicity of dynamic geophysical phenomena involving dynamic deformations of rocks (e.g. deformations such as those resulting from fast earthquake ruptures or from high-speed impact) need not only be interpreted by invoking electrokinetic mechanisms but can be generalized to all dielectrics that exhibit the flexoelectric phenomenon. In addition to dynamic geophysical phenomena, our generalized magneto-flexo-electric model is also appropriate for the modelling of dynamic rupture in many polymers such PMMA as Homalite-100 that are utilized in the "Laboratory Earthquake" set up, introduced by Rosakis and co-workers, (Xia et al., 2004; Rosakis et al., 2020). The fact that such materials, very much like various types of crustal rocks, are also strongly flexoelectric makes them excellent candidates as analogue materials to be used in the laboratory study of very fast earthquake ruptures. In particular, highly dynamic rupture processes, such as super-shear (or intersonic) rupture, are perfect candidates for analyzing by our dynamic magneto-flexo-electrictheory and eventually validating it through our analogue lab experiments.

The paper is structured as follows. In Section 2 we give a short account of our prior work in flexoelectricity regarding the mechanical displacements and the polarization. We then extend our prior work by formulating the governing equations for the electric and the magnetic fields that result from the polarization. In Section 3 we connect the electromagnetic potentials with the polarization potentials. In Section 4 we provide approximate solutions of the electric and the magnetic fields in terms of the acceleration and velocity fields. In Section 5 we establish an analogy between the magneto-flexo-electric formulation we established in Section 2 and the electrokinetic formulation used in fluid-saturated porous materials. In Section 6 we revisit the seismoelectric transfer functions found from the electrokinetic formulation and compare them with those found from the flexoelectric formulation in Section 4. In Section 7 we provide an analysis of plane wave propagation in flexoelectric and fluid-saturated porous materials. Finally, in Section 8 we synopsize our results and discuss important applications of the theory.

## 2. Magneto-flexo-electricity: the mechanical and the electromagnetic field

We examine a homogeneous linear flexoelectric solid (being dielectric at the same time) with an energy density due to elastic deformation and electric polarization which depends on the strain gradients. Reverse flexoelectricity implies that the gradient of the polarization produces strain and should be included in the energy density. The elastic strain energy due to strain gradient effects will not be considered and the kinetic strain energy will not include micro-rotational effects. We will first follow the approach of Giannakopoulos and Rosakis (2020) and decouple the problem to one that involves only the displacement vector (dynamic equation) and another that involves the polarization vector in relation to the displacement (transfer equation). Then, we will extend our previous theory by introducing a weak coupling with the electromagnetic field, as suggested by Mindlin and Toupin (1971). This will allow us to decouple the problems of electric and magnetic fields, which can be solved using the polarization found in the previous steps.

In what follows, consider the flexo-electric problem with key unknowns the material displacement vector $u_i$ [$m$], the material (electric) polarization vector $P_i$ [$C/m^2$] and the electric field $E_i$ [$Nm/C$]. These are functions of the (right-handed) Cartesian coordinates $x_1$, $x_2$, $x_3$ and the time $t$. The linear (Helmholtz) internal energy density function that includes deformation and polarization is (Maraganti et al., 2006; Sharma et al., 2010):

$$W = \begin{bmatrix} \frac{1}{2}a_{ij}P_iP_j + \frac{1}{2}b_{ijkl}P_{j,i}P_{l,k} + \frac{1}{2}c_{ijkl}\varepsilon_{ij}\varepsilon_{kl} + e_{ijkl}P_{j,i}\varepsilon_{kl} \\ +f_{ijkl}P_i\varepsilon_{kl,j} + b_{ij}^0P_{j,i} \end{bmatrix} \tag{2.1}$$

The mechanical linear strain is related to the displacement vector as $\varepsilon_{ij} = (u_{i,j} + u_{j,i})/2$. $P_{i,j}$ is the gradient of the polarization vector $P_i$ and $\varepsilon_{ij,k}$ are the gradients of the strains. Repeated indices imply summation from 1 to 3 and $()_{,i} = \partial/\partial x_i$. The dielectric body will be assumed to be a perfect insulator, so the divergent of the polarization vector is minus the bounded electric charge inside the body, $\nabla \cdot \overrightarrow{P} = -\rho_{bound}$[C/m³]. The compatibility equations are identical to classic linear elasticity. The form of the energy density function (2.1) omits an extra term that ensures thermodynamic stability of the total energy ($1/2g_{ijklmn} u_{i,jk} u_{l,mn}$). This term represents the contribution of purely elastic nonlocal effects. It has been found however (see Sharma et al., 2010) that, for most problems, excluding this contribution is generally small, although, if flexoelectricity is incorporated, it is required to guarantee thermodynamic stability. For some problems, this omission (or inclusion) of this term may be important especially where stability is an issue.

The material constants are: the elastic constant tensor $c_{ijkl}$ [$N/m^2$], the flexo-electric coefficient tensor $f_{ijkl}$ [$Nm/C$], the reciprocal dielectric susceptibility tensor $a_{ij}$ [$Nm^2/C^2$], the inverse flexo-electric coefficient tensor $e_{ijkl}$ [$Nm/C$] and the gradient polarization coupling tensor $b_{ijkl}$ [$Nm^4/C^2$]. The symmetries of the above constants have been addressed in (Shu et al., 2011). All these material tensors should be positive definite. The constants $b_{ij}^0$ are related to the surface energy per unit area $T_s = (n_i b_{ij}^0 P_j)/2$ with $n_i$ being the unit normal vector pointing outside the flexoelectric body (Mindlin, 1968) and do not affect the balance laws, but only the boundary conditions. The dielectric susceptibility $\chi$ relates to the dielectric constant of vacuum $\varepsilon_0$ as $1/a = \chi\varepsilon_0$. The classic elastic dielectric case is obtained, if $f_{ijkl} = 0$ and $e_{ijkl} = 0$, whereas the classic elastic case requires additionally $a_{ij} = 0$ and $b_{ij}^0 = 0$. If only $f_{ijkl} = 0$, we recover the formulation for a dielectric solid with polarization gradient. Typical material constants for PMMA (poly-methyl-methacrtylate) were estimated and are shown in Giannakopoulos and Rosakis (2020). A rather complete material data for alkali halides have been found by Askar et al. (1970) and for zirconia titanate by Zubko et al. (2008). Material data for single crystals can be estimated form atomistic

calculations, as for example by Maranganti and Sharma (2009).

In the works on continuum flexoelectricity so far, the Maxwell electric self-field$E_i$ was assumed to be furnished by an electric potential through $E_i = -\Phi_{,i}$ $[N/C]$. In this work, and in anticipation of the interaction with the magnetic field, we will eventually allow the electric field to be general. The total electric enthalpy is (Toupin, 1956):

$$\overline{H} = W - \frac{1}{2}\varepsilon_0 E_i E_i - E_i P_i \tag{2.2}$$

where, $\varepsilon_0 = 1/(36\pi) \times 10^{-9} \approx 8.854 \times 10^{-12} C^2 N^{-1} m^{-2} [= Fm^{-1}]$ is the dielectric permittivity of vacuum (assumed to surround the body). The weak interaction with the magnetic field is based on the assumption of the electric enthalpy as in (2.2), being essentially uncoupled to the magnetic field (Mindlin and Toupin, 1971). Later-on we will add the equations for the magnetic field $H_i$ (i.e. the Faraday's law, the Gauss' law and the Ampere's law) through the magnetic flux density vector$B_i [Nsm^{-1}C^{-1}=T]$. This approach implies the electric part of the Maxwell stress $\varepsilon_0(E_i E_j - 1/2\delta_{ij}E_k E_k)$ is less than the magnetic part of the Maxwell stress$(1/\mu_0)(B_i B_j - 1/2\delta B_k B_k)$, where$\mu_0 = 4\pi \times 10^{-7} kgm/C^2 [= Tm/A = H/m]$ is the magnetic permeability of vacuum and$\delta_{ij}$ is the Kronecker's delta. Therefore, the following inequalities must hold: $\varepsilon_0\mu_0 E_i E_i < B_k B_k$ and $\varepsilon_0\mu_0(E_i E_j)^2 < 4(E_k B_k)^2$. In most dielectrics, these assumptions are quite reasonable and their magnetic susceptibility can also be neglected. However, composites made of both magnetostrictive and piezo-electric compounds can exhibit strong electromagnetic coupling, see for example Nan (1994). Our present analysis excludes such composites.

The kinetic energy density is:

$$T = \frac{1}{2}\rho \dot{u}_i \dot{u}_i \tag{2.3}$$

where $\rho$ is the material mass density and $\dot{u}_i = \partial u_i/\partial t$ is the material velocity vector . If $\rho = 0$, the problem reduces to the static case. The constitutive relations, the balance equations, the boundary conditions and the initial conditions have been discussed by Giannako-poulos and Rosakis (2020) and are summarized here in Appendix A. Assuming zero body forces and initial electric field (or more generally for harmonic body forces and initial electric fields); we obtain the Cauchy-Navier type of governing equations:

$$c_{44}\nabla^2 \overrightarrow{u} + (c_{12} + c_{44})\nabla(\nabla \cdot \overrightarrow{u}) + (e_{44} - f_{12})\nabla^2 \overrightarrow{P} + (e_{12} + e_{44} - 2f_{44})\nabla(\nabla \cdot \overrightarrow{P}) = \rho \overset{..}{\overrightarrow{u}} \tag{2.4}$$

and

$$\begin{aligned}&(e_{44} - f_{12})\nabla \cdot \nabla^2 \overrightarrow{u} + (e_{12} + e_{44} - 2f_{44})\nabla^2\nabla \cdot \overrightarrow{u} \\ &+ (b_{44} + b_{77})\nabla \cdot \nabla^2 \overrightarrow{P} + (b_{12} + b_{44} - b_{77})\nabla^2\nabla \cdot \overrightarrow{P} - \left(a + \varepsilon_0^{-1}\right)\nabla^2\nabla \cdot \overrightarrow{P} = 0\end{aligned} \tag{2.5}$$

where,$\nabla^2 = \nabla_k\nabla_k = \partial^2/\partial x_1^2 + \partial^2/\partial x_2^2 + \partial^2/\partial x_3^2$ is the Laplacian operator, and $\nabla^4 = \nabla^2\nabla^2$ is the biharmonic operator. Note that the modified Eq. (2.5) has eliminated the electric field by incorporating the Gauss law, as shown in Appendix A.

The corresponding, work conjugate, boundary conditions are summarized in Table 1.

The initial conditions are: $u_i(\overrightarrow{x}, 0) = u_i^0(\overrightarrow{x}), \dot{u}_i(\overrightarrow{x}, 0) = \dot{u}_i^0(\overrightarrow{x}), P_i(\overrightarrow{x}, 0) = P_i^0(\overrightarrow{x})$ where $u_i^0$ is the initial displacement vector, $\dot{u}_i^0$is the initial velocity vector and $P_i^0$is the initial polarization vector and are often taken to be zero.

The representation of the general solution in the absence of body forces and initial electric field has been given by Giannakopoulos and Rosakis (2020) as a Helmholtz decomposition of both the displacement and the polarization vectors as

$$\overrightarrow{u} = \nabla\phi + \nabla \times \overrightarrow{H}^* \quad \nabla \cdot \overrightarrow{H}^* = 0 \tag{2.6}$$

**Table 1**
Mutually exclusive boundary conditions for the flexoelectric problem.

| Mutually Exclusive Boundary Conditions | |
|---|---|
| Essential Boundary Conditions | Dynamic Boundary Conditions |
| $P_i$ | $n_i E_{ij}$ |
| $\Phi$ | $n_i(\varepsilon_0\|E_i\| + \|P_i\|) = \sigma_s$ |
| | $E_i = -\Phi_{,i}$ |
| $Du_i$ | $r_i = \tau_{kji}n_k n_j$ |
| $u_i$ | $t_i = \sigma_{ij}n_j - \tau_{kji,k}n_j + (D_l n_l)n_j n_k\tau_{kji} - D_j(\tau_{kji}n_k)$ |

$n_i$is the unit normal vector pointing outside the body

$D \equiv n_k\partial/\partial x_k$ is the normal to the surface derivative

$D_j \equiv (\delta_{jk} - n_j n_k)\partial/\partial x_k$ is the tangential to the surface derivative

$\| \ \| = ()^+ - ()^-$ is the jump from outside of the body (+) to the inside of the body (-)

$\sigma_s$is the surface charge imposed on the dielectric boundary

$$\vec{P} = \nabla \chi^* + \nabla \times \vec{K} \quad \nabla \cdot \vec{K} = 0 \tag{2.7}$$

where $\phi(\vec{x}, t)$ and $\chi^*(\vec{x}, t)$ are scalar functions, whereas $\vec{H}^*(\vec{x}, t)$ and $\vec{K}(\vec{x}, t)$ are vector functions that are solutions of

$$\nabla^2 \phi - \ell_p^2 \nabla^4 \phi = \frac{1}{c_p^2} \left( \ddot{\phi} - h_p^2 \nabla^2 \ddot{\phi} \right) \tag{2.8}$$

$$\nabla^2 \vec{H}^* - \ell_s^2 \nabla^4 \vec{H}^* = \frac{1}{c_s^2} \left( \ddot{\vec{H}}^* - h_s^2 \nabla^2 \ddot{\vec{H}}^* \right) \tag{2.9}$$

$$\nabla^2 \chi^* - \ell_p^2 \nabla^4 \chi^* = \frac{1}{c_p^2} \left( \frac{e_{11} - f_{11}}{a + \varepsilon_0^{-1}} \nabla^2 \ddot{\phi} \right) \tag{2.10}$$

$$\nabla^2 \vec{K} - \ell_s^2 \nabla^4 \vec{K} = \frac{1}{c_s^2} \left( \frac{e_{44} - f_{12}}{a} \nabla^2 \ddot{\vec{H}}^* \right) \tag{2.11}$$

where the characteristic dilatation and shear speeds appear as it does in the classic elastodynamics

$$c_p = \sqrt{\frac{c_{11}}{\rho}} = \sqrt{\frac{c_{12} + 2c_{44}}{\rho}} = \sqrt{\frac{\lambda + 2\mu}{\rho}} = \sqrt{\frac{E(1 - \nu)}{\rho(1 + \nu)(1 - 2\nu)}}$$

$$\tag{2.12}$$

$$c_s = \sqrt{\frac{c_{44}}{\rho}} = \sqrt{\frac{\mu}{\rho}} = \sqrt{\frac{E}{2\rho(1 + \nu)}} < c_p$$

In the above equations $E$, and $\nu$ are the Young's modulus and the Poisson's ratio respectively, and $(\lambda, \mu)$ are the classic Lame constants. Moreover, four lengths appear, defined by

$$\{\mu, a, f_{12}, f_{44}, e_{44}, b_{44} + b_{77}, \mu(b_{44} + b_{77}) - e_{44}^2\} \rangle 0$$

$$\ell_s^2 = \frac{b_{44} + b_{77}}{a} - \frac{(e_{44} - f_{12})^2}{\mu a} \geq 0 \tag{2.13}$$

$$h_s^2 = \frac{(b_{44} + b_{77})}{a} \geq \ell_s^2 \geq 0$$

$$\{b_{11} = b_{12} + 2b_{44}, a, f_{11} = f_{12} + 2f_{44}, e_{11} = e_{12} + 2e_{44}, f_{44}, (\lambda + 2\mu)b_{11} - e_{11}^2\} \rangle 0$$

$$\ell_p^2 = \frac{b_{11}}{a + \varepsilon_0^{-1}} - \frac{(e_{11} - f_{11})^2}{(\lambda + 2\mu)(a + \varepsilon_0^{-1})} \geq 0 \tag{2.14}$$

$$h_p^2 = \frac{b_{11}}{a + \varepsilon_0^{-1}} \geq \ell_p^2 \geq 0$$

Eqs. (2.8) and (2.9) are the fundamental equations concerning only the mechanical fields, whereas Eqs. (2.10) and (2.11) are coupling equations that show how polarization fields couple with the mechanical fields. Thus, we obtain two "micro-structural" related lengths ($\ell_p, \ell_s$) and two "micro-inertial" related lengths ($h_p, h_s$). Note that the positiveness of the lengths stems from the assumed convexity of the energy density. Gradient dielectricity also yields the internal lengths ($\ell_p, \ell_s$) and ($h_p, h_s$), while flexo-electricity leads to higher microstructural lengths, compared to gradient dielectricity. The mechanical response is similar to the Mindlin's model of linear elastic solids with microstructure (Mindlin, 1963). We further note that polarization exhibits a size effect similar to the size effect of the mechanical displacement. The body forces and the initial electric fields may be easily incorporated in Eqs. (2.8-2.11) provided we can represent these fields as the displacement and polarization field in Eqs. (2.6) and (2.7). The general solution starts from the mechanical response, solving (2.8) for $\phi(\vec{x}, t)$, and (2.9) for $\vec{H}^*(\vec{x}, t)$. Once the displacement vector is found, the polarization vector can be found from the solution of (2.10) for $\chi^*(\vec{x}, t)$ and (2.11) for $\vec{K}(\vec{x}, t)$.

The dynamic response of polarization may lead to polarization acceleration that cannot be excluded if the present consideration is to be used to describe dynamic phenomena associated with impact and seismic events involving dynamic rupture. In these cases, the magnetic effects cannot be neglected. To incorporate them, we consider a Maxwell magnetic flux density vector $B_i[N/(Am) = Ns/(Cm) = Wb/m^2 = T]$ which acts both inside and outside of the material (the electric field acts inside the dielectric only). This, in turn, will create a magnetic field vector $H_i[A/m = C/(sm)]$. To find these fields, we follow the approach of Mindlin and Toupin (1971). Thus, the Maxwell equations specialize inside the body as follows:

$$\nabla \times \vec{E} + \dot{\vec{B}} = \vec{0} \tag{2.15}$$

which is a statement of Faraday's law and replaces the static law $\nabla \times \vec{E} = \vec{0}$. Next we include Gauss' law for magnetism (absent of free magnetic poles):

$$\nabla \cdot \vec{B} = 0 \tag{2.16}$$

Finally, we include Ampere's circuital law:

$$\nabla \times \vec{B} - \mu_0 \varepsilon_0 \dot{\vec{E}} - \mu_0 \dot{\vec{P}} = 0 \tag{2.17}$$

Furthermore, the quantity $\varepsilon_0 \vec{E} + \vec{P} = \vec{D}$ is defined as the total current density vector [A/m$^2$] and $\vec{D}$ [C/m$^2$] is the electric displacement vector. Note that $c_{light} = 1/(\varepsilon_0 \mu_0)^{1/2} \approx 3 \times 10^8 m/s$ is the speed of light in vacuum.

We now proceed to differentiate Eq. (2.17) once with respect to time, take the curl of Eq. (2.15) and then use the resulting equations to eliminate the magnetic flux density. Further use of the identity, $\nabla \times (\nabla \times \vec{E}) = \nabla(\nabla \cdot \vec{E}) - \nabla^2 \vec{E}$ allows us to obtain a relation between the electric field and the polarization as follow:

$$\nabla^2 \vec{E} - \nabla\left(\nabla \cdot \vec{E}\right) = \mu_0 \ddot{\vec{P}} + \mu_0 \varepsilon_0 \ddot{\vec{E}} \tag{2.18}$$

The above relation is a wave equation that can be solved for $\vec{E}$, provided that $\vec{P}$ (acting as a 'body force') is known and is obtained from the previous steps of the analysis. Once this is done, the magnetic flux $\vec{B}$ can be calculated from (2.15) and (2.16) and finally the magnetic field $\vec{H}$ [$A/m = C/ms$] can be estimated from a simple, linear constitutive equation that assumes isotropic dielectric material which cannot be magnetized, as follows:

$$\vec{H} \approx \mu_0^{-1} \vec{B} \tag{2.19}$$

These last steps of the solution require additional boundary conditions. As a matter of fact, these can be interface conditions with vacuum (referred to here as body 2) assumed to occupy the region exterior to the dielectric (referred to here as body 1) and are two for the electric field and two for the magnetic field (Born and Wolf; 1999 Jackson, 1975). These boundary conditions are shown in Appendix B.

It is also useful to derive the wave equation for the magnetic field $\vec{H}$. To achieve this, we take the curl of the Ampere's law (2.17) and differentiate it once with respect to time. We then utilize the constitutive Eq. (2.19) as well as Faraday's law (2.15). After some manipulation, we obtain:

$$\nabla^2 \vec{H} - \nabla\left(\nabla \cdot \vec{H}\right) = \mu_0 \nabla \times \dot{\vec{P}} + \mu_0 \varepsilon_0 \ddot{\vec{H}} \tag{2.20}$$

The above equation can be solved for $\vec{H}$, with known $\vec{P}$ (acting as a 'body force') from the previous steps of the analysis. Furthermore, we take the inner product of Faraday's law (2.15) with the magnetic flux $\vec{B}$. Then, we take the inner product of Ampere's law (2.17) with the electric field $\vec{E}$ and insert in it the previous result, while utilizing the identity $\nabla \cdot (\vec{E} \times \vec{B}) = (\nabla \times \vec{E}) \cdot \vec{B} - \vec{E} \cdot (\nabla \times \vec{B})$. Finally, by using the constitutive law (2.19) we replace the magnetic flux $\vec{B}$ with the magnetic field $\vec{H}$, and so we obtain the electromagnetic energy balance equation as follows:

$$-\nabla \cdot \left(\vec{E} \times \vec{H}\right) = \vec{H} \cdot \dot{\vec{B}} + \vec{E} \cdot \left(\varepsilon_0 \dot{\vec{E}} + \dot{\vec{P}}\right) \tag{2.20}$$

Note that in the above relation, $\vec{E} \times \vec{H}$ is the Poynting vector and that the product $\vec{E} \cdot (\varepsilon_0 \vec{E} + \vec{P})$ is called the Joule heat power. To the best of our knowledge, the relations (2.18), (2.20) and (2.21) have not been presented before in the context of flexoelectricity.

In summary, this section reviewed our previous results (2.4-2.14) and introduced a weak magnetic coupling that allowed us to formulate two new governing equations for the electric (2.18) and the magnetic (2.20) fields in relation to the polarization field. The mechanical and electromagnetic equations that control the problem can now be synopsized as follows:

$$\vec{u} = \nabla\phi + \nabla \times \vec{H}^*, \nabla \cdot \vec{H}^* = 0$$

$$\nabla^2\phi - \ell_p^2\nabla^4\phi = \frac{1}{c_p^2}\left(\ddot{\phi} - h_p^2\nabla^2\ddot{\phi}\right), \nabla^2\vec{H}^* - \ell_s^2\nabla^4\vec{H}^* = \frac{1}{c_s^2}\left(\ddot{\vec{H}}^* - h_s^2\nabla^2\ddot{\vec{H}}^*\right)$$

$$\vec{P} = \nabla\chi^* + \nabla \times \vec{K}, \nabla \cdot \vec{K} = 0 \hspace{4cm} + \mu_0\varepsilon_0\ddot{\vec{H}}$$

$$\nabla^2\chi^* - \ell_p^2\nabla^4\chi^* = \frac{1}{c_p^2}\left(\frac{e_{11} - f_{11}}{a + \varepsilon_0^{-1}}\nabla^2\ddot{\phi}\right), \nabla^2\vec{K} - \ell_s^2\nabla^4\vec{K} = \frac{1}{c_s^2}\left(\frac{e_{44} - f_{12}}{a}\nabla^2\ddot{\vec{H}}^*\right)$$

$$\nabla^2\vec{E} - \nabla\left(\nabla \cdot \vec{E}\right) = \mu_0\ddot{\vec{P}} + \mu_0\varepsilon_0\ddot{\vec{E}}, \nabla^2\vec{H} - \nabla\left(\nabla \cdot \vec{H}\right) = \mu_0\nabla \times \dot{\vec{P}}$$

## 3. The electromagnetic problem

In this section we will recast the electromagnetic problem stated at the end of Section 2 (Eqs. (2.18) and (2.20)), using electric potentials, as suggested by Mindlin (1974). Then we will replace the polarization vector with the polarization potentials found from our previous work. Following the classic work of Born and Wolf (1999), Eqs. (2.15-2.17) can be uniquely represented with a scalar electric potential $\Phi(\vec{x}, t)$ and a vector electric potential $\vec{A}(\vec{x}, t)$ so that:

$$\vec{E} = -\nabla\Phi - \dot{\vec{A}} = \vec{E}^p + \vec{E}^s \tag{3.1}$$

$$\vec{B} = \nabla \times \vec{A} \tag{3.2}$$

Eq. (3.2) satisfies Gauss Eq. (2.16) and Eq. (3.1) with (3.2) satisfy Faraday's Eq. (2.15) inside the body that develops polarization $\vec{P}(\vec{x}, t)$. Electromagnetism accepts a gauge condition and in the present work we accept the Lorentz condition $c_{light}^2 \nabla \cdot \vec{A} = -\dot{\Phi}$. The potentials $\Phi(\vec{x}, t)$ and $\vec{A}(\vec{x}, t)$ must satisfy the Ampere's Eq. (2.17). Inserting the representations (3.1) and (3.2) in (2.17) and using the Lorentz condition we obtain:

$$c_{light}^2\nabla^2\vec{A} - \ddot{\vec{A}} = -\varepsilon_0^{-1}\dot{\vec{P}} \tag{3.3}$$

Taking the divergence of (3.3) with the Lorentz condition and integrating once with respect to time, we obtain:

$$c_{light}^2\nabla^2\Phi - \ddot{\Phi} = \varepsilon_0^{-1}c_{light}^2\nabla \cdot \vec{P} \tag{3.4}$$

Taking into consideration the decomposition of the electric polarization $\vec{P}$ as in wq. (2.7), from (3.4) and (2.10) we obtain:

$$\nabla^2\Phi - \frac{1}{c_{light}^2}\ddot{\Phi} = \varepsilon_0^{-1}\nabla^2\chi^* \tag{3.5}$$

Subsequently, taking the curl of Eq. (3.3) into consideration with the decomposition of the electric polarization as of Eq. (2.11) we find that:

$$c_{light}^2\nabla^2\left(\nabla \times \vec{A}\right) - \nabla \times \ddot{\vec{A}} = -\varepsilon_0^{-1}\nabla \times \left(\nabla \times \dot{\vec{K}}\right) \tag{3.6}$$

Finally, assuming that the region exterior to the dielectric body is vacuum, then Eqs. (3.3) and (3.4) hold with $\vec{P}(\vec{x}, t) = \vec{0}$ and so we obtain $c_{light}^2\nabla^2\Phi = \ddot{\Phi}$ and $c_{light}^2\nabla^2\vec{A} = \ddot{\vec{A}}$.

In summary, in this section we recasted the electric and the magnetic field Eqs. (2.18) and (2.20) obtained in Section 2 in terms of two electric potentials (together with the Lorentz condition). Utilizing the piezoelectric potentials, we obtained the governing equations for the electric potentials in relation to the piezoelectric potentials and thus establishing the connection of the electromagnetic fileds with the flexoelectric problem.

## 4. The electromagnetic solution

In this section we construct the solution of (3.5) and (3.6) derived from Section 3 in terms of the mechanical velocities and accelerations. We start by noting that the velocity and the polarization rate can be stated from (2.6) and (2.7) as

$$\dot{\vec{u}} = \nabla\dot{\phi} + \nabla \times \dot{\vec{H}}^* = \dot{\vec{u}}^p + \dot{\vec{u}}^s \quad \nabla \cdot \dot{\vec{H}}^* = 0 \tag{4.1}$$

$$\dot{\vec{P}} = \nabla\dot{\chi}^* + \nabla \times \dot{\vec{K}} \quad \nabla \cdot \dot{\vec{K}} = 0 \tag{4.2}$$

Where $\vec{u}^p$ and $\vec{u}^s$ are displacements related to longitudinal p-waves and s-waves respectfully. For low frequencies, $\omega^2 / L << c_{light}^2$

where L is a characteristic, macroscopic length of the problem, or equivalently, for $V^2 << c_{light}^2$ where V is a characteristic velocity of the problem (e.g. the velocity of propagation of mechanical stress waves, or a crack tip velocity), we can assume $|\nabla^2 \Phi| >> |\ddot{\Phi}/c_{light}^2|$. Then (3.5) implies

$$\nabla^2 \Phi \approx \varepsilon_0^{-1} \nabla^2 \chi^* \tag{4.3}$$

which is approximately the electric balance equation in the absence of magnetic field. Taking as a first approximation $\ell_p^2 |\nabla^4 \chi^*| << |\nabla^2 \chi^*|$ the right hand side of (4.3) with Eq. (2.10) becomes $\varepsilon_0^{-1} \nabla^2 \chi^* \approx \frac{1}{c_p^2} \frac{e_{11} - f_{11}}{a\varepsilon_0 + 1} \nabla^2 \ddot{\phi}$. Recalling further that $\nabla \dot{\phi} = \vec{\dot{u}}_p$ and $\nabla \cdot (\nabla \ddot{\phi}) = \nabla^2 \ddot{\phi} = \nabla \cdot \vec{\ddot{u}}_p$, we obtain the approximation:

$$-\nabla \Phi = \vec{E}^p \approx -\frac{1}{c_p^2} \frac{e_{11} - f_{11}}{a\varepsilon_0 + 1} \vec{\dddot{u}}^p \tag{4.4}$$

This essentially means that the *solenoidal part of the electric field is proportional to the mechanical (dilatational) acceleration.* Using the data for PMMA from Giannakopoulos and Rosakis (2020), we obtain the ratio:

$$\frac{\left|\vec{\dddot{u}}^p\right|}{\left|\vec{E}^p\right|} \approx 225 \times 10^6 \frac{m^2}{s^2 V}$$

Taking representative values for alkali halides from Askar et al. (1970), we estimate:

$$\frac{\left|\vec{\dddot{u}}^p\right|}{\left|\vec{E}^p\right|} \approx 4.07 \times 10^6 \frac{m^2}{s^2 V}$$

Maranganti and Sharma (2009) provide flexoelectric data for periclase (magnesia), from which we estimate:

$$\frac{\left|\vec{\dddot{u}}^p\right|}{\left|\vec{E}^p\right|} \approx 7.54 \times 10^6 \frac{m^2}{s^2 V}$$

Using the material properties for ice from Petrenko (1993) with $c_p = 3800 \text{m/s}$ $e_{11} - f_{11} = 10 \text{V}, a\varepsilon_0 + 1 = 1.01$ we estimate:

$$\frac{\left|\vec{\dddot{u}}^p\right|}{\left|\vec{E}^p\right|} \approx 1.46 \times 10^6 \frac{m^2}{s^2 V}$$

Inside the flexo-electric material the magnetization current is zero, something quite true for dielectrics. The magnetization due to the magnetic flux is $\vec{M} = \chi_m \vec{B}/\mu_0$ (where $\chi_m$ is the magnetic susceptibility of the materials). The magnetization current is zero and so $\vec{J}_m = \nabla \times \vec{M} = \vec{0}$. Therefore $\nabla \times \vec{B} = \nabla \times (\nabla \times \vec{A}) = \vec{0}$ and so $\nabla \times (\nabla \times (\nabla \times \vec{A})) = -\nabla^2(\nabla \times \vec{A}) = \vec{0}$, and the magnetic flux is approximately harmonic $\nabla^2 \vec{B} = \nabla^2(\nabla \times \vec{A}) \approx \vec{0}$. Then we can approximate (3.6) as

$$\nabla \times \vec{\dddot{A}} \approx \varepsilon_0^{-1} \nabla \times \left(\nabla \times \vec{\dot{K}}\right) \tag{4.5}$$

We now integrate (4.5) with respect to time once, assuming zero initial conditions $(\vec{\dot{A}}(\vec{x}, t = 0) = \vec{K}(\vec{x}, t = 0) = \vec{0})$ and recall that since $\nabla \cdot \vec{K} = 0$ we have $\nabla \times (\nabla \times \vec{K}) = -\nabla^2 \vec{K}$. Then, (4.5) becomes

$$\nabla \times \vec{\ddot{A}} \approx -\varepsilon_0^{-1} \nabla^2 \vec{K} \tag{4.6}$$

With the approximation $\ell_s^2 |\nabla^4 \vec{K}| << |\nabla^2 \vec{K}|$ and Eq. (2.11), Eq. (4.6) with (4.1) and (3.1) becomes

$$\nabla \times \vec{\ddot{A}} + \varepsilon_0^{-1} \frac{1}{c_s^2} \left(\frac{e_{44} - f_{12}}{a}\right) \nabla^2 \vec{\dddot{H}}^* = -\nabla \times \vec{\dot{E}}^s + \varepsilon_0^{-1} \frac{1}{c_s^2} \left(\frac{e_{44} - f_{12}}{a}\right) \nabla^2 \vec{\ddot{H}} \approx \vec{0} \tag{4.7}$$

We now integrate the left-hand side of (4.7) with respect to time once, assuming zero initial conditions $(\vec{A}(\vec{x}, t = 0) = \vec{\dot{H}}(\vec{x}, t = 0) = \vec{0})$. Since $\nabla \cdot \vec{H}^* = 0$, we have $\nabla \times (\nabla \times \vec{\dot{H}}^*) = -\nabla^2 \vec{\dot{H}}^* = \nabla \times \vec{\dot{u}}^s$. Then using (3.2) and the constitutive law (2.19) we obtain (with $c_{light}^2 = 1/(\varepsilon_0 \mu_0)$):

$$\vec{H} \approx \frac{c_{light}^2}{c_s^2} \left(\frac{e_{44} - f_{12}}{a}\right) \nabla \times \vec{\dot{u}}^s \tag{4.8}$$

Obviously then, *the magnetic flux and the magnetic field are proportional to the curl of the mechanical (shear) velocity.*

Taking the data for PMMA from Giannakopoulos and Rosakis (2020), we estimate:

$$\frac{\left|\overrightarrow{H}\right|}{|\nabla \times \overrightarrow{u}^s|} = 5.361 Cm^{-1}$$

Taking the data for the minerals Tausonite (SrTiO$_3$) and Macedonite (PbTiO$_3$) from Giannakopoulos and Zisis(2021), we estimate:

$$\frac{|\overrightarrow{H}|}{|\nabla \times \overrightarrow{u}^s|} = 180.0 Cm^{-1} \text{ and } \frac{|\overrightarrow{H}|}{|\nabla \times \overrightarrow{u}^s|} = 510.0 Cm^{-1} \text{ respectively}$$

Taking the data for the mineral periclase (magnesia), from Maranganti and Sharma (2009), we estimate:

$$\frac{\left|\overrightarrow{H}\right|}{|\nabla \times \overrightarrow{u}^s|} = 1169 Cm^{-1}$$

Taking the shear velocity of ice 1934 m/s and the flexoelectric data similar to the longitudinal values, we obtain $\frac{|H|}{|\nabla \times \overrightarrow{u}^s|} = 21.28 Cm^{-1}$.

In summary, in this section we showed the (approximate) connections of the electric and magnetic fields with the shear accelerations and the dilatation velocities, respectively, through the novel Eqs. (4.4) and (4.8). These important approximations connect the electromagnetic problem with the mechanical problem in the context of flexoelectricity. Finally, we gave some numerical estimates for materials and minerals for which sufficient material data exist.

## 5. Analogy with the electro-magnetic field of the electrokinetic theory

In this section we will prove an interesting analogy between the electromagnetic equations derived in the Section 2 for the flexoelectricity theory (Eqs. (2.18) and (2.20)) and the electromagnetic fields deduced by the well-established electrokinetic theory developed for fluid-saturated porous materials which is used extensively in geosciences. Pride and his coworkers (Pride, 1994; Pride and Haardsen, 1996; Pride and Garambois, 2005) established the modern electro kinetic theory which is a combination of a mechanical field developed by a fluid saturated porous material (non-magnetic dielectric mineral) and the Maxwell electromagnetic field. The solid and fluid phases are treated separately following the well-known theory of Biot in the context of what is called poroelasticity (see for example Biot (1962)).

The coupling between the electromagnetic and the poroelastic response is established by transfer functions relating the small current (called electro filtration) that is allowed due to the electro kinetic coupling with the gradient of the fluid pressure $\nabla p_f$ and the solid phase acceleration multiplied by the fluid density $\rho_f \ddot{\overrightarrow{u}}_{solid}$ (results that come from poroelasticity). The physical ground of the electro kinetics is the Stern's electric double layer that forms between the fluid and the solid walls. Therefore, the total current $\overrightarrow{J}^{pe}$ is found by adding the electro kinetic current $L_0(-\nabla p_f + \rho_f \ddot{\overrightarrow{u}}_{solid})$ with the usual Ohm's current $\overline{\phi}\sigma_f \overrightarrow{E}^{pe}/\alpha_\infty$ (the constants are the fluid density $\rho_f [kgm^{-3}]$, the fluid electric conductivity $\sigma_f [Sm^{-1} = CV^{-1}s^{-1}]$, the porosity $\overline{\phi}$ and and the (electric) tortuosity of the pores $\alpha_\infty$). On the other hand, the Darcy filtration velocity $\overrightarrow{w}$ (which comes from poroelasticity), also couples with the electric field $\overrightarrow{E}^{pe}$ through the same electro kinetic parameter $L_0 [CmN^{-1}s^{-1}]$ (Onsager theorem) with the electric field creating what is called electro-osmosis, $L_0 \overrightarrow{E}^{pe}$. If $L_0 = 0$, then there is no electro kinetic coupling between the mechanical and the electrical problem. Otherwise, the total filtration velocity adds the influence of electro-osmosis to the standard Darcy's law $(\eta_f/k_f)(-\nabla p_f + \rho_f \ddot{\overrightarrow{u}}_{solid})$ (the constants are the fluid kinematic viscosity $\eta_f [Pas]$ and the fluid permeability $k_f [m^2]$). The initial full development of the theory of Pride was given in the frequency space since most of the many parameters that appear are functions of the frequency.

As a start, we will omit the mechanical equilibrium and the constitutive laws of (linear and isotropic) poroelasticity, assuming that the poroelastic problem will communicate its results, namely the fluid pressure, the solid phase velocity and the filtration velocity $(\overrightarrow{w}, p_f, \overrightarrow{u}_{solid})$. We will focus on the two Maxwell equations (with basic unknowns the electric $\overrightarrow{E}^{pe}$ and the magnetic field $\overrightarrow{H}^{pe}$) together with the two transfer equations for the electric current $\overrightarrow{J}^{pe}$ and the filtration velocity $\overrightarrow{w}$. The equations will be stated in the real time domain, assuming that the involved parameters take their steady-state values. This simplifying assumption holds good for frequencies below the transition frequency of Biot $\omega < \omega_t = \overline{\phi}\eta_f/(\alpha_\infty k_f \rho_f)$, implying the dominance of the viscous forces over the inertial forces of the fluid motion. Determination of rock properties by low-frequency AC electro kinetics can be found in (Pengra et al., 1999) among others. The electro-kinetic transfer equations are as follows:

$$\overrightarrow{J}^{pe} = L_0\left(-\nabla p_f + \rho_f \overrightarrow{g}_0 + \rho_f \ddot{\overrightarrow{u}}_{solid}\right) + \frac{\overline{\phi}}{\alpha_\infty}\sigma_f \overrightarrow{E}^{pe} \tag{5.1}$$

$$\dot{\overrightarrow{w}} = \frac{k_f}{\eta_f}\left(-\nabla p_f + \rho_f \overrightarrow{g}_0 + \rho_f \ddot{\overrightarrow{u}}_{solid}\right) + L_0 \overrightarrow{E}^{pe} \tag{5.2}$$

The superscript pe stands for poro-elastic. Note that the original relations of Pride (1994) did not include the contribution of a

constant acceleration field $\vec{g}_0$, e.g. Earth's gravity 9.81 m/s$^2$. Next we state the Maxwell equations (Faraday's and Ampere's respectively) as formulated by the electro kinetic theory:

$$\nabla \times \overrightarrow{H}^{pe} = \varepsilon_0 \left( \frac{\overline{\phi}}{\alpha_\infty} \left( \varepsilon_f - \varepsilon_s \right) + \varepsilon_s \right) \dot{\overrightarrow{E}}^{pe} + \overrightarrow{J}^{pe} + \frac{\overline{\phi}}{\alpha_\infty} \sigma_f \dot{\vec{w}} \times \overrightarrow{B}_0 \tag{5.3}$$

$$\nabla \times \overrightarrow{E}^{pe} = -\mu_0 \dot{\overrightarrow{H}}^{pe} \tag{5.4}$$

where the new constants are the dielectric constant (relative permittivity) of the fluid $\varepsilon_f$ and the dielectric constant of the solid phase $\varepsilon_s$. Note that the constant magnetic flux $\overrightarrow{B}_0$ is assumed to pre-exist (e.g Earth's magnetic flux which is about 0.32 μT, atmospheric magnetic flux etc). Therefore, the last term of (5.3) describes an electromotive force due to the fluid motion.

The electro-kinetic problem defined by Pride (1994) involves through the electro-kinetic parameter $L_0 [Cm N^{-1} s^{-1}]$ two internal lengths, the Deby screening length $d [m]$ and a length that has to do with the electric response of the fluid inside the pores of the material $\Lambda [m]$ and is of the order of the pore radius. The electrokinetic parameter reads as:

$$L_0 = -\frac{\overline{\phi}}{\alpha_\infty} \frac{\varepsilon_0 \varepsilon_f \zeta}{\eta_f} \left( 1 - \frac{2d}{\Lambda} \right) \approx -\frac{\overline{\phi}}{\alpha_\infty} \frac{\varepsilon_0 \varepsilon_f \zeta}{\eta_f} = -C_{ef} \sigma_f \tag{5.5}$$

Eq. (5.5) introduces a new parameter, the zeta potential $\zeta [V]$ that describes the electric field at the solid-fluid interface (typically -20 $\times 10^{-3}$ V). A thorough account of the zeta potential can be found in (Reppert et al., 2001). The constant $C_{ef} [V/Pa]$ is the electro filtration parameter that was introduced by various authors (see for example (Revil et al., 1999)) and is a quantity that can be measured (electric potential difference vs pressure difference) in place of the combination of other constants that are difficult to access. The Deby length (about $3 \times 10^{-10}$m) has been discussed thoroughly by Revil and Glover (1998) among others and is typically much less than the pore diameter $2d << \Lambda$. Walker and Glover (2010) relate the value of $\Lambda$ with the porosity $\overline{\phi}$, the grain radius $r_{grain}$ and the electrical cementation exponent $m$ (typically $m$=1.5), according to

$$\Lambda \approx \frac{\overline{\phi}^m}{m} r_{grain} \tag{5.6}$$

and estimate it to be of order 40-80 $\times 10^{-6}$m.

We condense the above equations, aiming to develop a wave equation with respect to the electric field $\overrightarrow{E}^{pe}$ and the filtration velocity $\vec{w}$. First we eliminate $(-\nabla p_f + \rho_f \overrightarrow{g}_0 + \rho_f \ddot{\vec{u}}_{solid})$ from (5.1) and (5.2) and obtain:

$$\nabla^2 \overrightarrow{E}^{pe} - \nabla \nabla \cdot \overrightarrow{E}^{pe} = \mu_0 \frac{\eta_f L_0}{k_f} \ddot{\vec{w}} + \mu_0 \frac{\overline{\phi}}{\alpha_\infty} \sigma_f \ddot{\vec{w}} \times \overrightarrow{B}_0 + \mu_0 \varepsilon_0 \left( \frac{\overline{\phi}}{\alpha_\infty} (\varepsilon_f - \varepsilon_s) + \varepsilon_s \right) \ddot{\overrightarrow{E}}^{pe}$$
$$+ \mu_0 \left( \frac{\overline{\phi}}{\alpha_\infty} \sigma_f - \frac{\eta_f L_0^2}{k_f} \right) \dot{\overrightarrow{E}}^{pe} \tag{5.7}$$

Eq. (5.7) is a (linear) wave equation for the electric field with the last term describing a 'diffusion' effect for the electric field. Excluding this last term (which is true for small porosity), the rest of the equation resembles our flexoelectric Eq. (2.18), provided we accept a polarization vector of the form

$$\overrightarrow{P} \to \frac{\eta_f L_0}{k_f} \vec{w} + \frac{\overline{\phi}}{\alpha_\infty} \sigma_f \vec{w} \times \overrightarrow{B}_0 \tag{5.8}$$

a relative electric permittivity from the solid-fluid composite

$$\varepsilon_0 \to \varepsilon_0 \left( \frac{\overline{\phi}}{\alpha_\infty} (\varepsilon_f - \varepsilon_s) + \varepsilon_s \right) \tag{5.9}$$

and the mappings

$$\overrightarrow{E} \to \overrightarrow{E}^{pe} \\ \overrightarrow{H} \to \overrightarrow{H}^{pe} \tag{5.10}$$

Next, we eliminate $(-\nabla p_f + \rho_f \overrightarrow{g}_0 + \rho_f \ddot{\vec{u}}_{solid})$ from (5.1) and (5.2) and obtain:

$$\nabla^2 \overrightarrow{H}^{pe} - \nabla \left( \nabla \cdot \overrightarrow{H}^{pe} \right) = \mu_0 \frac{\eta_f L_0}{k_f} \nabla \times \dot{\vec{w}} + \mu_0 \frac{\overline{\phi}}{\alpha_\infty} \sigma_f \nabla \times \left( \dot{\vec{w}} \times \overrightarrow{B}_0 \right) + \mu_0 \varepsilon_0 \left( \frac{\overline{\phi}}{\alpha_\infty} (\varepsilon_f - \varepsilon_s) + \varepsilon_s \right) \ddot{\overrightarrow{H}}^{pe}$$
$$+ \mu_0 \left( \frac{\overline{\phi}}{\alpha_\infty} \sigma_f - \frac{\eta_f L_0^2}{k_f} \right) \dot{\overrightarrow{H}}^{pe} \tag{5.11}$$

Eq. (5.11) is a (linear) wave equation for the magnetic field with the last term describing a 'diffusion' effect for the magnetic field,

analogous to that found in the electric field (5.7). Excluding this last term (which is true for small porosity), the rest of the equation has a remarkable resemblance to our flexoelectric Eq. (2.20), provided we accept the analogy already found for the electric field (5.8), (5.9) and (5.10). Fig. 1 shows schematically *the basic analogy between* $\overrightarrow{P}$ *and* $\overrightarrow{w}$*, implied by Eq. (5.8)*. Typical values of $L_0$ for unconsolidated soils is $0.7 \times 10^{-8} m^2 s^{-1} V^{-1}$. The pressure gradient in earthquakes is $10^{+2} - 10^{+4} N/m^3$ and Eq. (5.1) provides electrical currents of the order $10^{-6} - 10^{-4} A/m^2$.

Therefore, (5.8), (5.9) and (5.10) establish the fascinating analogy of the flexoelectric problem with the electro kinetic problem, as far as the electromagnetic fields are concerned. It is interesting to point the direct connection of the flexoelectric polarization vector $\overrightarrow{P}$ with the electrokinetic filtration vector $\overrightarrow{w}$. Also note that flexoelectric polarization still exist, even if the electro kinetic coupling constant is absent from (5.8), thus covering models that tend to ignore the pure electro kinetic effect $L_0 = 0$. All aforementioned constants can be directly measured or estimated from particular analyses.

Omitting the "diffusion" terms of Eqs. (5.7) and (5.11) raises the issue of how much dissipation energy is neglected relative to the flexoelectric electric energy balance. Pride and Haartsen (1996) have found the electromagnetic energy balance as

$$-\nabla \cdot \left( \overrightarrow{E}^{pe} \times \overrightarrow{H}^{pe} \right) = \overrightarrow{H}^{pe} \cdot \dot{\overrightarrow{B}}^{pe} + \overrightarrow{E}^{pe} \cdot \left( \dot{\overrightarrow{D}}^{pe} + \overrightarrow{J}^{pe} + \frac{\overline{\phi}}{\alpha_\infty} \sigma_f \dot{\overrightarrow{w}} \times \overrightarrow{B}_0 \right) \tag{5.12}$$

with $\overrightarrow{D}^{pe} = \varepsilon \overrightarrow{E}^{pe}$. Comparing (5.12) with (2.21) and taking into account (5.8), (5.9) and (5.10), we conclude that there is an additional energy rate term on the right hand side of (5.12). Subtracting (2.20) from (5.12) we obtain the dissipation energy rate as:

$$-\nabla \cdot \left( \overrightarrow{E}^{pe} \times \overrightarrow{H}^{pe} \right) + \nabla \cdot \left( \overrightarrow{E} \times \overrightarrow{H} \right) = \overrightarrow{E}^{pe} \cdot \overrightarrow{E}^{pe} \left( \frac{\overline{\phi}}{\alpha_\infty} \sigma_f - \frac{\eta_f L_0^2}{k_f} \right) \tag{5.13}$$

which for low porosity $(\overline{\phi} < 1)$ is very small. A characteristic 'diffusion' time emerges from Eqs. (5.7) and (5.11), utilizing (5.5):

$$t_d = \frac{\varepsilon_0 \left( \frac{\overline{\phi}}{\alpha_\infty} \left( \varepsilon_f - \varepsilon_s \right) + \varepsilon_s \right)}{\frac{\overline{\phi}}{\alpha_\infty} \left( \sigma_f + \frac{\left( \varepsilon_0 \varepsilon_f \zeta \right)^2}{\eta_f k} \right)} \tag{5.14}$$

For typical values of the constants, the order of this time scale is extremely small ($10^{-7}$ s), indicating a fast diffusion process for the electromagnetic field inside the porous material.

In summary, in this section we have proven a remarkable novel analogy between the electromagnetic results of the flexoelectric theory and the electromagnetic results of the electrokinetic theory, provided we ignore the small diffusion term present in the electrokinetic theory (the flexoelectric theory did not include dissipative terms). The analogy is established by recognizing the similarity between the polarization and the fluid filtration velocity through quations (5.8-5.10). In this respect, the electric and magnetic fields
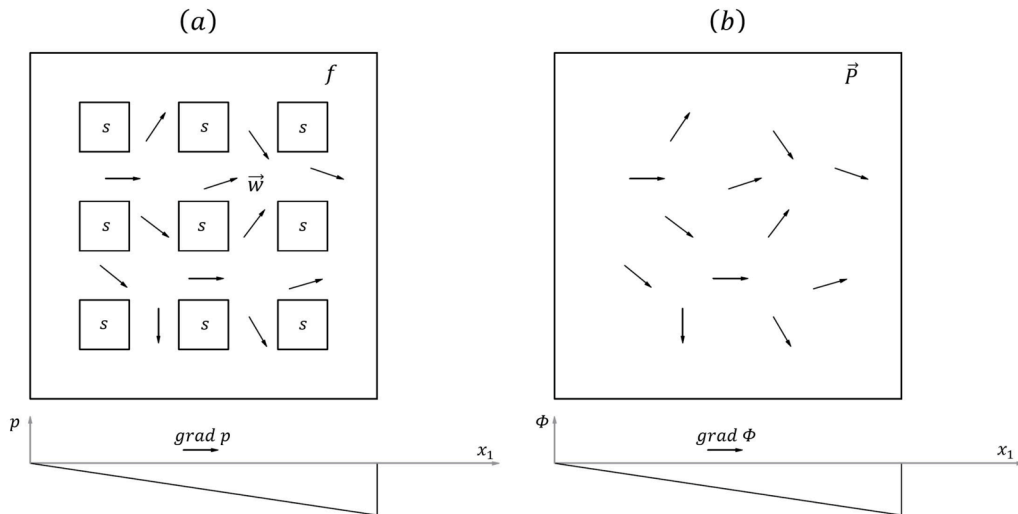


**Fig. 1.** A simple schematic showing the basic electro-magnetic analogy between (a) a *poroelastic material* with electrokinetic coupling and (b) a *flexoelectric material*. The solid grains of the poroelastic materials (s) are shown schematically as squares with the fluid phase (f) flowing around them. The connectivity of the fluid channels is far more complex than what is shown in the schematic. The poroelastic material under a *gradient of the fluid pressure* $p_f$, develops the *fluid infiltration velocity field* $\overrightarrow{w}$ between the solid grains of the material. The flexoelectric material under a *gradient of the electric potential* $\Phi$ develops an *electric field* $\overrightarrow{E}$ hence and a *polarization field* $\overrightarrow{P}$. In the absence of electro-magnetic and mechanical body forces the two vector fields $(\overrightarrow{w}, \overrightarrow{P})$ are *proportional*.

are similar in both theories: Eq. (5.7) with (2.18) and Eq. (5.11) with (2.20).

## 6. Seismoelectric transfer functions

In this section we will review the application of Pride's electrokinetic theory in the analysis of coseismic electromagnetic fields that are observed in earthquakes. The outcome is the connection between the electric field and the dilatation acceleration and between the magnetic field and the curl of the shear velocity. What is of interest to us is the analogies with the flexoelectric results given by Eqs. (4.4) and (4.8) derived in Section 4. In doing so, we will provide relations between the material constants used in electrokinetics and the material constants used in flexoelectricity.

Bordes et al. (2015) based on Pride's results (see section 5) found the low frequency expression of the coseismic seismoelectric field (under harmonic response) as:

$$\vec{E}^{pe} = \vec{E}^{p} + i\vec{E}^{s} \tag{6.1}$$

That is the electric filed breaks into an in-phase field that related to the P-waves and an out of phase (at $\pi/2$ angle) field related to the S-waves, with the in phase electric field to dominate. Bordes et al. (2015) estimate that

$$\vec{E}^{p} \approx -C_{ef}\rho_f \left(1 - \frac{\rho_t}{\rho_f}\frac{C}{H}\right)\ddot{\vec{u}}^p \tag{6.2}$$

The new parameters in (6.2) are the $C$ and $H$ [Pa] elastic moduli of Biot (1962), which have been discussed in various publications and its ratio can usually be neglected ($C/H < 1$), and the average material density $\rho_t = \overline{\phi}\rho_f + (1 - \overline{\phi})\rho_s$. An equation similar to (6.2) was found first by Garambois and Dietrich (2001). The shear related electric field was estimated by Bordes et al. (2015) to be

$$\vec{E}^{s} \approx C_{ef}\rho_f \frac{\mu_0}{\omega}\frac{\overline{\phi}}{\alpha_\infty}\frac{G}{\rho_t}\sigma_f \ddot{\vec{u}}^s \tag{6.3}$$

Note that the result (6.3) depends on the frequency $\omega$. Both approximations (6.2) and (6.3) were found to be exact for frequencies below a critical value:

$$\omega < \frac{\overline{\phi}\eta_f}{\alpha_\infty k_f \rho_f} \tag{6.4}$$

According to our flexoelectric analogue, Eq. (6.2) has the same form as our Eq. (4.4), provided we map the flexoelectric constants as:

$$\frac{1}{c_p^2}\frac{e_{11} - f_{11}}{a\varepsilon_0 + 1} \rightarrow C_{ef}\rho_f \left(1 - \frac{\rho_t}{\rho_f}\frac{C}{H}\right) \tag{6.5}$$

Next, assume that the magnetic field is due to the shear part of the electric potential. Then, Ampere's law (5.4) is satisfied by taking the curl of (6.3) and so

$$\dot{\vec{H}}^{pe} \approx -\mu_0^{-1}\nabla \times \vec{E}^{s} \approx -C_{ef}\rho_f \frac{1}{\omega}\frac{\overline{\phi}}{\alpha_\infty}\frac{G}{\rho_t}\sigma_f \nabla \times \dddot{\vec{u}}^s \tag{6.6}$$

Integrating (6.6) once with respect to time assuming zero initial conditions for the velocity and the magnetic field, we obtain

$$\vec{H}^{pe} \approx -C_{ef}\rho_f \frac{1}{\omega}\frac{\overline{\phi}}{\alpha_\infty}\frac{G}{\rho_t}\sigma_f \nabla \times \dot{\vec{u}}^s \tag{6.7}$$

Eq. (6.7) has the same form as Eq. (4.8), provided we map the flexoelectric constants according to

$$\frac{c_{light}^2}{c_s^2}\left(\frac{e_{44} - f_{12}}{a}\right) \rightarrow -C_{ef}\rho_f \frac{1}{\omega}\frac{\overline{\phi}}{\alpha_\infty}\frac{G}{\rho_t}\sigma_f \tag{6.8}$$

Hence, the flexoelectric analogue provides two relations between the constants of flexoelectricity and the electro kinetic poroelasticity, (6.5) and (6.8).

Regarding the magnetic field transfer equation, we point at another estimate proposed by Garambois and Dietrich (2001),

$$\left|\vec{H}^{pe}\right| \approx \rho_f \frac{\overline{\phi}}{\alpha_\infty}\frac{\varepsilon_0\varepsilon_f|\zeta|}{\eta_f}\sqrt{\frac{G}{\rho_t}}|\dot{\vec{u}}^s| \tag{6.9}$$

For harmonic responses, Eq. (6.9) is similar to Eq. (6.7), if we note from (5.5) that $-\frac{\overline{\phi}}{\alpha_\infty}\frac{\varepsilon_0\varepsilon_f\zeta}{\eta_f} = -C_{ef}\sigma_f$, that the gradient operator corresponds in the frequency domain to multiplication with the wave number $k$, and that $k/\omega \approx \sqrt{\rho_t/G}$.

It is interesting to examine the relative magnitude of the flexoelectric constants under the prism of the analogy with the electrokinetic equivalents (6.5) and (6.8). Their ratio is given by

$$\frac{\chi}{\chi+1}\frac{e_{11}-f_{11}}{e_{44}-f_{12}} \rightarrow -\omega\frac{\varepsilon_0}{\sigma_f}\frac{\alpha_\infty}{\overline{\overline{\phi}}}\left(1-\frac{\rho_t}{\rho_f}\frac{C}{H}\right)\frac{c_{light}^2 c_p^2}{c_s^4} \tag{6.10}$$

Typical values of the parameters on the right hand side of (6.10) and for low values of frequency lead to the conclusion that

$$\frac{\chi}{\chi+1}\frac{e_{11}-f_{11}}{e_{44}-f_{12}} >> 1 \tag{6.11}$$

This result and the results of (2.13) and (2.14) necessitates the conclusion $\ell_s \approx h_s$ while $\ell_p < h_p$. In the context of the problem of supershear ruptures propagating in flexoelectric materials (e.g. PMMA or Rocks) and the experimental observation of both shear and dilatational Mach lines at their tips discussed in the introduction (Rosakis et al., 2020; Gori et al., 2018), the observation that $\ell_s \approx h_s$ means that the *shear type of Mach lines would have a slope similar to that predicted by classical elastodynamics where gradient effects are neglected*. On the other hand the fact that, $\ell_p < h_p$,will generally hold, means that *the dilatational type of Mach lines have a slope less than that predicted by classical elastodynamics* as is shown by the fast rupture experiments performed in PMMA and as theoretically explained by Giannakopoulos and Rosakis (2020) .

We now examine a specific example of sea ice that can be assessed from both flexoelectric and electrokinetic models. Williams and Francois (1991) suggested that ice can be mechanically viewed as a Biot solid with very small water porosity. They measured the p-wave velocity and mass density as functions of temperature and salinity, typical values are$c_p \approx 3800 m/s, \rho_f \approx 1000 kg/m^3$. Drzymala et al. (1999) measured the ice/water zeta potential as a function of the PH of the water, a typical value is$\zeta \approx -27V$. Artemov (2019) estimated the electrical conductivity of the brine, a typical value is$\sigma_f \approx 3.1 \times 10^{-3} S/m$. Finally, the dynamic viscosity of brine is$3 \times 10^{-3} Pas$ and the dielectric constant of ice is$\chi + 1 \approx 100$. Then Eq. (6.3) gives$e_{11} - f_{11} \approx 40V$, which is comparable to the value of 10V estimated by Evtushenko et al. (1987).

Garambois and Dietrich (2001) report measurements of unconsolidated porous medium with different levels of salinity to be in the range:

$$\frac{\left|\ddot{\vec{u}}^p\right|}{\left|\vec{E}^p\right|} \approx 171 - 717 \frac{m^2}{s^2 V}$$

This result is lower than the results found for flexoelectric materials (see Section 4). On some other results from (Bordes et al., 2008) for saturated Fontainebleau sand and frequency $\omega = 1s^{-1}$, we estimate:

$$\frac{\left|\vec{H}^{pe}\right|}{\left|\nabla \times \dot{\vec{u}}^s\right|} = 1.466 Cm^{-1}$$

From (Bordes et al., 2015) for saturated silica sand and frequency$\omega = 1s^{-1}$, we obtain:

$$\frac{\left|\vec{H}^{pe}\right|}{\left|\nabla \times \dot{\vec{u}}^s\right|} = 0.02689 Cm^{-1}$$

This number is of the same order of magnitude as that found from (Garambois and Dietrich, 2001) who have employed an entirely different approach. These results are comparable to those we found for flexoelectric materials (see Section 4).

In summary, we have shown that the flexoelectric analogy with the electrokinetic theory can be used for the analytic and experimental investigation of the coseismic electromagnetic emissions of earthquakes, provided that the material constants can be mapped according to the novel Eqs. (6.5) and (6.8). These relations are of great importance for the laboratory investigations of earthquakes, because flexoelectric materials can be utilized as analogue materials in the experiments.

## 7. Plane waves in homogeneous, isotropic flexoelectric and poroelastic materials

In this section we provide an application of previous results in the context of plane waves. Consider dilatational polarization plane waves in homogeneous flexoelectric materials. The electric field can be derived from Eq. (4.4) and drives a zero net current. Therefore it does not create a magnetic field. We then investigate shear plane waves and assume, without loss of generality, a shear plane wave that propagates in the $x_1$ direction ($x_1$, $x_2$, $x_3$ the Cartesian reference system) of the form:

$$u_2^s(\xi) = u_2^s(x_1 - \overline{c}_s t)$$

$$u_3^s(\xi) = u_3^s(x_1 - \overline{c}_s t) \tag{7.1}$$

The shear wave speed$\overline{c}_s$ can be obtained by inserting Eq. (7.1) into Eq. (2.9) and observing that the higher derivatives can be eliminated with a shear wave speed$\overline{c}_s = c_s(\ell_s/h_s)$. Since$\ell_s/h_s \le 1$, we have$\overline{c}_s \le c_s$, that is the shear wave speed can be slower than the classic one. A similar analysis can be performed with a dilatational plane wave of the form$u_1^p(\xi) = u_1^p(x_1 - \overline{c}_p t)$, which can be inserted in Eq. (2.8) and provide a dilatation wave speed$\overline{c}_p = c_p(\ell_p/h_p)$. Since$\ell_p/h_p \le 1$ also in this case, we have$\overline{c}_p \le c_p$, that is the dilatation wave speed can be slower than the classic one.

Replacing Eq. (7.1) into (4.7) and into (4.8), we obtain respectively the approximate forms:

$$\frac{E_2^s}{H_3} \approx \frac{-\ddot{u}_2^s}{\partial \dot{u}_2^s / \partial x_1} \mu_0 = \mu_0 \bar{c}_s$$

$$\frac{E_3^s}{H_2} \approx \frac{-\ddot{u}_3^s}{-\partial \dot{u}_3^s / \partial x_1} \mu_0 = -\mu_0 \bar{c}_s$$

(7.2)

The same results as (7.2) will be obtained, if we replace Eq. (7.1) into the poroelastic estimates (6.2) and (6.7) respectively.

Now consider dilatational harmonic plane waves in homogeneous poroelastic materials. The electric field can be derived from Eq. (6.2) and drives a zero net current. Therefore it does not create a magnetic field. Assume next, without loss of generality, a shear harmonic plane wave that propagates in the $x_1$ direction with slowness $s_s = 1/\bar{c}_s$. The shear displacements are:
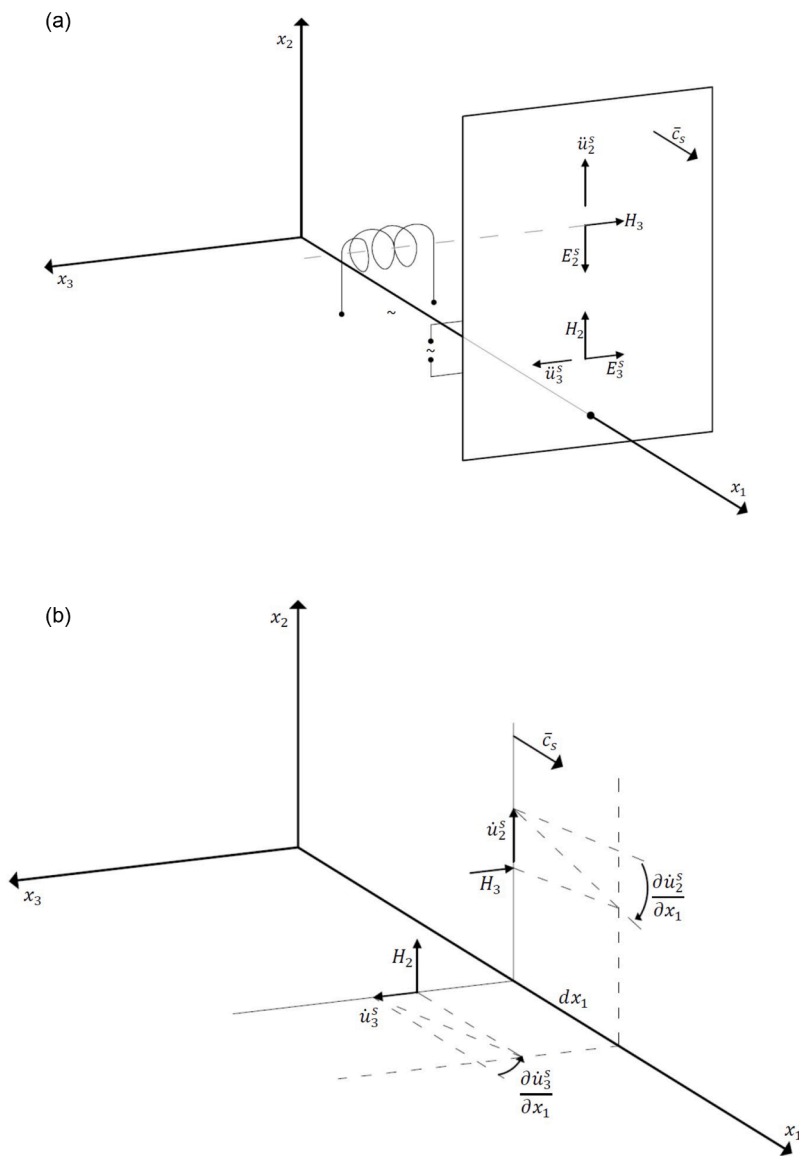


Fig. 2. A *shear plane wave*, traveling with velocity $\bar{c}_s = c_s(\ell_s / h_s)$ in the $x_1$–direction. (a) The shear electric field vector $(E_2^s, E_3^s)$ is analogous and opposite of the acceleration vector $(\ddot{u}_2, \ddot{u}_3)$. (b) The velocity curl vector $(-\partial \dot{u}_3^s / \partial x_1, \partial \dot{u}_2^s / \partial x_1)$ creates the magnetic field vector $(H_2, H_3)$ analogous to the velocity curl.

$$u_2^s = u_2^{s0} \exp[-i\omega(t - s_s x_1)]$$

$$u_3^s = u_3^{s0} \exp[-i\omega(t - s_s x_1)]$$

$$(7.3)$$

In this case, due to the relative fluid-solid motion, a streaming current $J_1^{pe}$ will be generated. This current will induce a magnetic field with components $H_2^{pe}$ and $H_3^{pe}$ which are orthogonal to the wave (and current) direction, according to Ampere's law. The magnetic components are given by Eq. (6.7) with

$$\frac{\partial}{\partial x_1} \dot{u}_2^s = u_2^{s0} \omega^2 s_s \exp[-i\omega(t - s_s x_1)]$$

$$\frac{\partial}{\partial x_1} \dot{u}_3^s = u_3^{s0} \omega^2 s_s \exp[-i\omega(t - s_s x_1)]$$

$$(7.4)$$

Thus, the magnetic field moves inside the shear plane and, due to Faraday's law, it will create an electric field. The corresponding electric field has $E_2^s$ and $E_3^s$ components that can be derived from Eq. (6.3) with

$$\ddot{u}_2^s = -u_2^{s0} \omega^2 \exp[-i\omega(t - s_s x_1)]$$

$$\ddot{u}_3^s = -u_3^{s0} \omega^2 \exp[-i\omega(t - s_s x_1)]$$

$$(7.5)$$

Therefore, magnetic activity is expected only for shear shock waves and electric activity is expected for both shear and dilatation waves.

The relation between the components of the electric and the magnetic field can be easily computed, giving the simple relations:

$$\frac{E_2^s}{H_3} = \frac{-\ddot{u}_2^s}{\partial \dot{u}_2^s / \partial x_1} \mu_0 = \mu_0 \frac{1}{s_s} = \mu_0 \bar{c}_s$$

$$\frac{E_3^s}{H_2} = \frac{-\ddot{u}_3^s}{-\partial \dot{u}_3^s / \partial x_1} \mu_0 = -\mu_0 \frac{1}{s_s} = -\mu_0 \bar{c}_s$$

$$(7.6)$$

The same results as Eq. (7.6) will be obtained, if we replace (7.3) into the flexoelectric estimates (4.7) and (4.8) respectively. The shear wave velocity of many rocks is of the order of $3000 m/s$, see (Simmons, 1964). This means that the ratio of the electric to the magnetic field as predicted by Eq. (7.6) is of the order of $0.4 \times 10^{-2} V/A$. Mizutani et al. (1976) estimated that the electric fields were of the order of $0.7 \times (10^{-6} - 10^{-3}) V/m$, whereas the magnetic fields were of the order of $1.6 \times (10^{-4} - 10^{-1}) A/m$, with their ratio falling within the prediction of Eq. (7.6).

We conclude that the same ratios of the electric to the magnetic fields were found for both the flexoelectric and the poroelastic materials, as expected from the electric analogy we have established. On this plane, the shear part of the electric field $E_2^s$ in the $x_2$-direction generates a magnetic field $H_3$ in the $x_3$-direction. The shear part of the electric field $E_3^s$ in the $x_3$-direction generates a magnetic field $H_2$ in the $x_2$-direction. Fig. 2a shows the shear electric field vector $(E_2^s, E_3^s)$, which is analogous and opposite of the acceleration vector $(\ddot{u}_2, \ddot{u}_3)$. Fig. 2b shows the velocity curl vector $(-\partial \dot{u}_3^s / \partial x_1, \partial \dot{u}_2^s / \partial x_1)$ that creates the magnetic field vector $(H_2, H_3)$ analogous to the velocity curl. A properly located magnetometer (e.g. a coil directed in a magnetic field axis) can measure the magnetic field and a properly located potentiometer (e.g. electrodes attached along an electric field axis) can measure the electric field, as shown in Fig. 2a. Magnetic fields can be carried along by mechanical shear waves only. This is illustrated in Fig. 2 which shows a shear plane wave, traveling with velocity $\bar{c}_s$ in the $x_1$-direction.

## 8. Conclusions

We have extended the flexoelectric analysis in an uncoupled electromagnetic theory and found that the electric field is proportional to the dilatation mechanical (particle) acceleration and the magnetic flux and the magnetic field are proportional to the mechanical (particle) velocity. Remarkably, our theory seems to be analogous to the electro kinetic poroelasticity theory of Pride which is based on an entirely different set of assumptions and has been used to assess seismo-magnetic phenomena and measurements. We have established an electric analogue through the flexoelectric response, by representing the relative fluid-grain velocity with the flexo-electric polarization that depends on the mechanical strain gradients. The rate of the electric displacement of flexoelectricity replaces the streaming current of electro kinetic poroelasticity. Physically, at a microscopic level, the two models have in common the combined electrons and ions that in flexoelectricity come from polarization due to strain gradient and in porous materials come from wetting fluids that form electric double layers in the porous channels. The analogy is completed upon recognition that the diffusion effect of the electric field (due to the viscosity of poroelasticity) is often small.

The novel aspects of our present analysis can be summarized in the following relations:

(a) The governing equations of the electric field (2.18) and the magnetic field (2.20) based on the polarization vector found from our previous work.

(b) The connection of the electrodynamic potentials with the polarization potentials through Eqs. (3.5) and (3.6).

(c) The approximate solutions for the electric (4.4) and the magnetic (4.8) fields as functions of the dilatational acceleration and the curl of the shear velocity, respectively.

(d) The corresponding mappings (5.8-5.10) that establish the analogy of the flexoelectric theory with the electrokinetic theory of wetted porous materials.

(e) The mappings (6.5) and (6.8) that establish the relation between the material properties used in the flexoelectric theory and the electrokinetic theory for wetted porous materials.

In addition to rocks (e.g. sandstone, marble, limestone), ice and other material systems of importance to geophysics, the results are also important for all dielectrics such as ceramics, perovskites and polymers that exhibit strong flexoelectric effect, often uncoupled from piezoelectricity (centrosymmetric materials). Moreover, our conclusions also apply to certain nano-composites and atomistic models that can be approached in the context of couple stress elasticity. In such cases, the origin of the micro-structural and micro-inertial lengths is very different that the one proposed in this work.

Flexoelectricity is currently used in many applications, and in particular in energy harvesting devices that collect electric energy, using the electric fields that are created from mechanical vibrations and then harvested by surface attached electrodes, see for example Deng et al. (2014), Deng and Shen (2018), Mura and Erturk (2017). For a recent review on flexoelectric energy harvesting technology see Tripathy et al. (2021). However, the magnetic aspects of flexoelectricity are far less exploited in device applications, let alone analytical and numerical investigations. We believe that our present work will serve as a building step for flexoelectric applications that involve the ensuing magnetic fields such as remotely operating sensors and actuators, nanocompasses and nanocoils, Giannakopoulos and Rosakis (2022).

**CRediT authorship contribution statement**

**Antonios E. Giannakopoulos:** Conceptualization, Methodology, Investigation, Writing – original draft, Writing – review & editing, Formal analysis. **Ares J. Rosakis:** Conceptualization, Methodology, Investigation, Writing – original draft, Writing – review & editing, Formal analysis.

**Declaration of Competing Interest**

The authors declare that they have no known competing financial interests or personal relationships that could have appeared to influence the work reported in this paper.

**Data availability**

Data will be made available on request.

**Appendix A**

The flexoelectric constitutive equations are:

a Cauchy (symmetric) stress tensor:

$$\sigma_{ij} = \frac{\partial W}{\partial \varepsilon_{ij}} = c_{ijkl}\varepsilon_{kl} + e_{klij}P_{l,k}$$

b Dipolar stress tensor:

$$\tau_{ijk} = \frac{\partial W}{\partial \varepsilon_{jk,i}} = f_{lijk}P_l$$

c Effective local electric force:

$$\overline{E}_k = -\frac{\partial W}{\partial P_k} = -\left(a_{kj}P_j + f_{klij}\varepsilon_{ij,l}\right)$$

d Polarization gradient force:

$$E_{ij} = \frac{\partial W}{\partial P_{j,i}} = b_{ijkl}P_{l,k} + e_{ijkl}\varepsilon_{kl} + b_{ij}^0$$

We will concentrate in the isotropic response and in this case the constitutive property tensors become:

$$a_{ij} = a\delta_{ij}$$

$$c_{ijkl} = c_{12}\delta_{ij}\delta_{kl} + c_{44}\left(\delta_{ik}\delta_{jl} + \delta_{jk}\delta_{il}\right)$$

$$f_{ijkl} = f_{12}\delta_{ij}\delta_{kl} + f_{44}\left(\delta_{ik}\delta_{jl} + \delta_{jk}\delta_{il}\right)$$

$$e_{ijkl} = e_{12}\delta_{ij}\delta_{kl} + e_{44}\left(\delta_{ik}\delta_{jl} + \delta_{jk}\delta_{il}\right)$$

$$b_{ijkl} = b_{12}\delta_{ij}\delta_{kl} + b_{44}\left(\delta_{ik}\delta_{jl} + \delta_{jk}\delta_{il}\right) + b_{77}\left(\delta_{ik}\delta_{jl} - \delta_{jk}\delta_{il}\right)$$

$$b_{ij}^0 = b_0\delta_{ij}$$

where $\delta_{ij}$ is Kronecker's delta (identity tensor). Using Hamilton's principle (least action), that is minimizing the total electric enthalpy with respect to $u_i$ and $P_i$ in the whole body volume V and for arbitrary time interval $(0, t_1)$,

$$\int_0^{t_2} \int_V \delta(\overline{H} - T)dVdt = 0$$

we obtain the Euler conditions for all the material points of the body (in the presence of body forces $X_i$ [N/m$^3$] and initial electric field $E_i^0$ [N/C]):

a  Conservation of linear momentum:

$$\sigma_{ji,j} - \tau_{kji,jk} + X_i = \rho\ddot{u}_i$$

b  Conservation of electric field:

$$\overline{E}_j + E_{ij,i} + E_j + E_j^0 = 0$$

c  Gauss' law (absence of free charges) inside the body:

$$\varepsilon_0 E_{i,i} + P_{i,i} = 0$$

d  Maxwell-Faraday (static) equations outside the body of perfect insulators in absence of magnetic flux:

$$\nabla \times \overrightarrow{E} = \overrightarrow{0}$$

where $\nabla$ is the gradient operator, or, using the alternating Levi-Civita tensor, $\varepsilon_{ijk}E_{k,j} = 0$. This last equation defines a potential $\Phi$, so that $E_i = -\Phi_{,i}$.

Assuming zero body forces and initial electric field $(X_i = 0[N/m^3]$, $E_i^0 = 0[N/C])$ in the conservation of linear momentum and conservation of electric field, we obtain the two Cauchy-Navier types of equations:

$$c_{44}\nabla^2 u_i + (c_{12} + c_{44})\nabla_i(\nabla_k u_k) + (e_{44} - f_{12})\nabla^2 P_i + (e_{12} + e_{44} - 2f_{44})\nabla_i(\nabla_k P_k) = \rho\ddot{u}_i$$

$$(e_{44} - f_{12})\nabla^2 u_i + (e_{12} + e_{44} - 2f_{44})\nabla_i(\nabla_k u_k) + (b_{44} + b_{77})\nabla^2 P_i + (b_{12} + b_{44} - b_{77})\nabla_i(\nabla_k P_k)$$
$$-aP_i + E_i = 0$$

supplemented by the Gauss law:

$$\varepsilon_0 E_{i,i} + P_{i,i} = 0$$

where $\nabla^2 = \nabla_k\nabla_k = \partial^2/\partial x_1^2 + \partial^2/\partial x_2^2 + \partial^2/\partial x_3^2$ is the Laplacian operator, $\nabla^4 = \nabla^2\nabla^2$ is the biharmonic operator. Note that, if $f_{ijkl} = 0, e_{ijkl} = 0$ and $a_{ij} = 0$, we obtain the classic elastodynamic equations. The above three partial differential equations are the initial governing equations of the flexoelectric problem regarding the mechanical displacement field $\overrightarrow{u}$ and the polarization field $\overrightarrow{P}$.

By taking the divergent of the second Cauchy-Navier type equation and using Gauss equation, we eliminate the electric field to

obtain:

$$(e_{44} - f_{12})\nabla \cdot \nabla^2 \overrightarrow{u} + (e_{12} + e_{44} - 2f_{44})\nabla^2 \nabla \cdot \overrightarrow{u}$$
$$+ (b_{44} + b_{77})\nabla \cdot \nabla^2 \overrightarrow{P} + (b_{12} + b_{44} - b_{77})\nabla^2 \nabla \cdot \overrightarrow{P} - \left(a + \varepsilon_0^{-1}\right)\nabla^2 \nabla \cdot \overrightarrow{P} = 0$$

Thus the reformulation of the problem leads to solving two coupled equations with respect to the displacement vector $u_i$ and the polarization vector $P_i$ from the two condensed governing equations:

$$c_{44}\nabla^2 \overrightarrow{u} + (c_{12} + c_{44})\nabla(\nabla \cdot \overrightarrow{u}) + (e_{44} - f_{12})\nabla^2 \overrightarrow{P} + (e_{12} + e_{44} - 2f_{44})\nabla(\nabla \cdot \overrightarrow{P}) = \rho \ddot{\overrightarrow{u}}$$

$$(e_{44} - f_{12})\nabla \cdot \nabla^2 \overrightarrow{u} + (e_{12} + e_{44} - 2f_{44})\nabla^2 \nabla \cdot \overrightarrow{u}$$
$$+ (b_{44} + b_{77})\nabla \cdot \nabla^2 \overrightarrow{P} + (b_{12} + b_{44} - b_{77})\nabla^2 \nabla \cdot \overrightarrow{P} - \left(a + \varepsilon_0^{-1}\right)\nabla^2 \nabla \cdot \overrightarrow{P} = 0$$

## Appendix B

As discussed in the main text in detail, the solution for $\overrightarrow{P}$ from the above equations allows us to solve for the magnetic flux $\overrightarrow{B}$ and the electric field $\overrightarrow{E}$ within the context of weak magnetic interaction by using the following relations:

$$\nabla \times \overrightarrow{E} + \dot{\overrightarrow{B}} = \overrightarrow{0}$$

$$\nabla \cdot \overrightarrow{B} = 0$$

$$\nabla \times \overrightarrow{B} - \mu_0 \varepsilon_0 \dot{\overrightarrow{E}} - \mu_0 \dot{\overrightarrow{P}} = 0$$

with appropriate boundary conditions. Let $\overrightarrow{n}$ be the unit vector normal to the dielectric (body 1) pointing outside the body. Then from the integral form of Faraday's law we have the condition:

$$\overrightarrow{n} \times \left(\overrightarrow{E}^{(2)} - \overrightarrow{E}^{(1)}\right) = \overrightarrow{0}$$

If a known surface free charge density $\sigma_s$ [C/m$^2$] is applied through adsorption on the dielectric body:

$$\overrightarrow{n} \cdot \left(\overrightarrow{D}^{(2)} - \overrightarrow{D}^{(1)}\right) = \sigma_s$$

where the electric displacement field is defined by $\overrightarrow{D} = \varepsilon_0 \overrightarrow{E} + \overrightarrow{P}$.

From the integral form of Gauss' law for magnetism (absence of free magnetic poles) we have the condition:

$$\overrightarrow{n} \cdot \left(\overrightarrow{B}^{(2)} - \overrightarrow{B}^{(1)}\right) = 0$$

From the integral form of the Ampere's law, if a known surface free current density $\overrightarrow{j}_s$ [A/m$^2$] is applied through electrodes attached on the dielectric body, we have:

$$\overrightarrow{n} \times \left(\overrightarrow{H}^{(2)} - \overrightarrow{H}^{(1)}\right) = \overrightarrow{j}_s$$

The electric boundary conditions can be materialized with appropriate steady state currents applied by surface conductors.

## References

Aki, K., Richards, P.G., 1980. Qualitative Seismology, 2. Freeman and Company, New York. W.H.

Amlani, F., et al., 2022. Supershear shock front contributions to the tsunami from the 2018 Mw 7.5 Palu earthquake. Geophys. Res. Lett. 230, 2089–2097 accepted.

Artemov, V.G., 2019. A unified mechanism for ice and water electrical conductivity from direct current to terahertz. Phys. Chem. Chem. Phys. R. Soc. Chem. https://doi.org/10.1039/C9CP00257J.

Askar, A., Lee, P.C.Y., Cakmak, A.S., 1970. Lattice-dynamics approach to the theory of elastic dielectrics with polarization gradient. Phys. Rev. B 1, 3525–3537.

Bao, H., et al., 2019. Early and persistent supershear rupture of the 2018 magnitude 7.5 Palu earthquake. Nat. Geosci. 12, 200–205.

Biot, M.A., 1962. Mechanics of deformation and acoustic propagation in porous media. J. Phys. 33, 1482–1498.

Bordes, C., et al., 2008. Evidence of the theoretically predicted seismo-magnetic conversion. Geophys. J. Int. 174, 489–504.

Bordes, C., et al., 2015. Impact of water saturation on seismoelectric transfer functions: a laboratory study of coseismic phenomenon. Geophys. J. Int. 200, 1317–1335.

Born, M., Wolf, E., 1999. Principles of Optics, 7th ed. Cambridge University Press.

Bouchon, M., et al., 2001. How fast is rupture during an earthquake? New insights from the 1999 Turkey earthquakes. Geophys. Res. Lett. 28, 2723–2726.

Deng, Q., Kammoun, M., Erturk, A., Sharma, P., 2014. Nanoscale flexoelectric energy harvesting. Int. J. Solids Struct. 51, 3218–3224.

Deng, Q., Lv, S., Li, Z., Tan, K., Liang, X., Shen, S., 2020. The impact of flexoelectricity on materials, devices and physics. J. Appl. Phys. 128, 080902.

Deng, Q., Shen, S., 2018. The flexodynamic effect on nanoscale flexoelectric energy harvesting: a computational approach. Smart Mater. Struct. 27, 105001.

Draganov, A.B., Inan, U.S., Taranenko, Y.M., 1991. ULF magnetic signatures at the earth surface due to ground water flow: a possible precursor to earthquakes. Geophys. Res. Lett. 18, 1127–1130.

Drzymala, J., Sadowski, Z., Holysz, L., Chibowski, E., 1999. Ice/water interface: zeta potential, point of zero charge and hydrophobicity. J. Colloid Interface Sci. 220, 229–234.

Elbanna, A., et al., 2021. Anatomy of strike-slip fault tsunami genesis. PNSA 118, 19e2025632118. No.

Ellsworth, W., et al., 2004. Near-field ground motion of the 2002 Denali fault, Alaska, earthquake recorded at pump station 10. Earthq. Spectra 20, 597–615.

Enomoto, Y., Yanab, T., Okumura, N., 2017. Causal mechanism of seismo-EM phenomena during the 1965-1967 Matsushiro earthquake swarm. Sci. Rep. 7, 44774.

Evtushenko, A.A., Maeno, N., Petrenko, V.F., Ryzhkin, I.A., 1987. Pseudopiezoelectric effects in ice. J. Phys. 48, 113.

Fifolt, D.D., Petrenko, V.F., Schulson, E.M., 1993. Preliminary study of electromagnetic emissions from cracks in ice. Philos. Mag. Part B 67, 289–299.

Gakhberg, M.B., Morgounov, V.A., 1982. Experimental measurement of electromagnetic emissions possibly related to earthquakes in Japan. J. Geophys. Res. 87, 7824–7828.

Garambois, S., Dietrich, M., 2001. Seismoelectric wave conversions in porous media: field measurements and transfer functional analysis. Geophysics 66, 1417–1430.

Gavardinas, I.D., Giannakopoulos, A.E., Zisis, T.H., 2018. A von Karman plate analogue for solving anti-plane problems in couple stress and dipolar gradient elasticity. Int. J. Solids Struct. 148-149, 169–180.

Giannakopoulos, A.E., Zisis, T.H., 2019. Uniformly moving screw dislocation in flexoelectric materials. Eur. J. Mech. A Solids 78, 103843.

Giannakopoulos, A.E., Zisis, T.H., 2021. Uniformly moving antiplane cracks in flexoelectric materials. Eur. J. Mech. A Solids 85, 104136.

Giannakopoulos, A.E., Rosakis, A.J., 2020. Dynamics of flexoelectric materials: subsonic, intersonic and supersonic ruptures and Mach cone formation. J. Appl. Mech. ASME 87, 061004, 1/9.

Giannakopoulos, A.E., Rosakis, A.J., 2022. Creating magnetic micro/nanodevices from flexoelectric materials, Provisional patent application as filed by. California Institute of Technology CIT File No.: CIT-8823-P.

Gori, M., Rubino, V., Rosakis, A.J., Lapousta, N., 2018. Pressure shock fronts formed by ultra-fast shear cracks in viscoelastic materials. Nat. Commun. 9, 4754.

Gugliemi, A.V., Tsegmed, B., Potapov, A.S., Kultima, J., Raita, T., 2006. Seismomagnetic signals from the strong Sumatra earthquake. Izv. Phys. Solid Earth 42, 921–927.

Honkura, Y., et al., 2009. A model for observed circular polarized electric fields coincident with the passage of large seismic waves. J. Geophys. Res. 114, B10103.

Hu, T., Yang, W., Liang, X., Shen, S.P., 2018. Wave propagation in flexoelectric microstructured solids. J. Elast. 130, 197–210.

Hu, S.L., Shen, S.P., 2009. Elastic field gradient theory with surface effect for nano-dielectrics. Comput. Mater. Contin. 13, 63–87.

Ida, Y., Aki, K., 1972. Seismic source time function of propagating longitudinal-shear cracks. J. Geophys. Res. 77, 2034–2044.

Ishido, T., Mizutani, H., 1981. Experimental and theoretical basis of electrokinetic phenomena in rock-water systems and its applications to geophysics. J. Geophys. Res. 86, 1763–1775.

Jackson, J.D., 1975. Classical Electrodynamics. John Willey & Sons, New York.

Jiang, X., Huang, W., Zhang, S., 2013. Flexoelectric nano-ganerator: materials, structures and devices. Nano Energy 2, 1079–1092.

Johnston, M.J.S., Sasai, Y., Egbert, G.D., Mueller, R.J., 2006. Seismomagnetic effects from the long-awaited 28 September 2004 M6.0 Parkfield earthquake. Bull. Seismol. Soc. Am. 96, S206–S220.

Jouniaux, L., Zyserman, F., 2016. A review on electrokinetically induced seismo-magnetics for earth sciences. Solid Earth 7, 249–284.

Krichen, S., Sharma, P., 2016. Flexoelectricity: a perspective on an unusual electromechanical coupling. J. Appl. Mech. 83, 030801.

Liu, C., Lambros, J., Rosakis, A.J., 1993. Highly transient elastodynamic crack growth in a bi-material interface: higher order asymptotic analysis and optical experiments. J. Mech. Phys. Solids 41, 1887–1954.

Majdoub, M.S., Sharma, P., Cagin, T., 2008. Enhanced size-dependent piezoelectricity and elasticity in nanostructures due to the flexoelectric effect. Phys. Rev. B 77, 125424.

Maranganti, R., Sharma, N.D., Sharma, P., 2006. Electromechanical coupling in non-piezoelectric materials due to nanoscale nonlocal size effects: Green's functions and embedded inclusions. Phys. Rev. B 74, 014110. Erratum: Piezoelectric thin-film super-lattices without using piezoelectric materials [J. Appl. Phys. 108, 024304 (2010)] N. D. Sharma, C. Landis, and P. Sharma.

Maranganti, R., Sharma, P., 2009. Atomistic determination of flexoelectric properties of crystalline dielectrics. Phys. Rev. B 80, 054109.

Matsushima, M., et al., 2002. Seismo-electromagnetic effect associated with the Izmit earthquake and its aftershocks. Bull. Seismol. Soc. Am. 92, 350–360.

Mindlin, R.D., 1963. Micro-structure in linear elasticity. Arch. Ration. Mech. Anal. 16, 51–78.

Mindlin, R.D., 1968. Polarization gradient in elastic dielectric. Int. J. Solids Struct. 4, 637–642.

Mindlin, R.D., Toupin, R.A., 1971. Acoustical and optical activity in alpha quartz. Int. J. Solids Struct. 7, 1219–1227.

Mindlin, R.D., 1974. Electromagnetic radiation from a vibrating, elastic sphere. Int. J. Solids Struct. 10, 1307–1314.

Mizutani, H., Ishido, T., Yokokura, T., Ohnishi, S., 1976. Electrokinetic phenomena associated with earthquakes. Geophys. Res. Lett. 3, 365–368.

Mizutani, H., Ishido, T., 1976. A new interpretation of magnetic field variation associated with the Matsushiro earthquakes. J. Geomagn. Geoelectr. 28, 179–188.

Mura, A., Erturk, A., 2017. Electroelastodynamics of flexoelectric energy conversion and harvesting in elastic dielectrics. J. Appl. Phys. 121, 064100.

Nan, C.W., 1994. Magnetoelectric effect in composites of piezoelectric and piezomagnetic phases. Phys. Rev. B 50, 6082–6088.

Ogawa, T., Oike, K., 1985. Electromagnetic radiation from rocks. J. Geophys. Res. 90, 6245–6249.

Pengra, D.B., Li, X.S., Wong, P., 1999. Determination of rock properties by low-frequency AC electrokinetics. J. Geophys. Res. 104, 29485–29508.

Petrenko, V.F., 1993. On the nature of electrical polarization of materials caused by cracks. Applications to ice electromagnetic emissions. Philos. Mag. B 67, 301–315.

Pride, S., 1994. Governing equations for the coupled electromagnetics and acoustics of porous media. Phys. Rev. B 50, 15678.

Pride, S.R., Haartsen, M.W., 1996. Electroseismic wave properties. J. Acoust. Soc. Am. 100, 1301–1315.

Pride, S.R., Garambois, S., 2005. Electroseismic wave theory of Frenkel and more recent developments. J. Eng. Mech. 131, 898–907.

Ren, H., Wen, J., Huang, Q., Chen, X., 2015. Electrokinetic effect combined with surface-charge assumption: a possible generation mechanism of coseismic EM signals. Geophys. J. Int. 200, 835–848.

Reppert, P.M., Morgan, F.D., Lesmes, D.P., Jouniaux, L., 2001. Frequency-dependent streaming potentials. J. Colloid Interface Sci. 234, 194–203.

Revil, A., Glover, P.W.J., 1998. Nature of surface electrical conductivity in natural sands, sandstones, and clays. J. Geophys. Res. 104, 20021–20031.

Revil, A., Pezard, P.A., Glover, P.W.J., 1999. Streaming potential in porous media 1. Theory of the zeta potential. J. Geophys. Res. 104, 20021–20031.

Rosakis, A.J., Samudrala, O., Coker, D., 1999. Cracks faster than the shear wave speed. Science 284, 1337–1340.

Rosakis, A.J., Rubino, V., Lapusta, N., 2020. Recent milestones in unravelling the full-field structure of dynamic shear cracks and fault ruptures in real time: from photoelasticity to ultrahigh-speed digital image correlation. J. Appl. Mech. 87, 030801.

Sharma, N.D., Landis, C.M., Sharma, P., 2010. Piezoelectric thin-film superlattices without using piezoelectric materials. J. Appl. Phys. 108, 024304.

Shen, S.P., Hu, S.L., 2010. A theory of flexoelectricity with surface effect for elastic dielectrics. J. Mech. Phys. Solids 58, 665–677.

Shu, L., Wei, X., Pang, T., Yao, X., Wang, C., 2011. Symmetry of flexoelectric coefficients in crystalline medium. J. Appl. Phys. 110, 104106.

Simmons, G., 1964. Velocity of shear waves in rocks to 10 kilobars. J. Geophys. Res. 69, 1123–1130.

Tagantsev, A.K., 1991. Electric polarization in crystals and its response to thermal and elastic perturbations. Phase Transit. 35, 119–203.

Toupin, R.A., 1956. The elastic dielectric. J. Ration. Mech. Anal. 5, 849–915.

Tripathy, A., Saravanakumar, B., Mohanty, S., Nayak, S.K., Ramadoss, A., 2021. Comprehensive review on flexoelectric energy harvesting technology: mechanisms, device configurations, and potential applications. Appl. Electron. Mater. 3, 2898–2924.

Ujihara, N., Honkura, Y., Ogawa, Y., 2004. Electric and magnetic field variations arising from the seismic dynamo effect for after-shocks of the M7.1 earthquake of 26 May 2003 off Miyagi prefecture, NE Japan. Earth Planets Space 56, 115–123.

Walker, F., Glover, P.W.J., 2010. Permeability models of porous media: characteristic length scales, scaling constants and time-dependent electrokinetic coupling. Geophysics 75, E235–E246.

Wang, B., Gu, Y., Zhang, S., Chen, L.Q., 2019. Flexoelectricity in solids: progress, challenges and perspectives. Prog. Mater. Sci. 106, 100570.

Williams, K.L., Fransois, R.E., 1991. Sea ice elastic moduli: determination of Biot parameters using in-field velocity measurements. J. Acoust. Soc. Am. https://doi.org/10.1121/1.402970.

Xia, K., Rosakis, A.J., Kanamon, H., 2004. Laboratory earth quakes: THE sub-Rayleigh-to-supershear rupture transition. Science 303, 1859–1861.

Yamada, I., Masuda, K., Mizutani, H., 1989. Electromagnetic and acoustic emission associated with rock fracture. Phys. Earth Plenary Inter. 57, 157–168.

Yoshida, S., Clint, O.C., Sammonds, P.R., 1998. Electric potential charges prior to shear fracture in dry and saturated rocks. Geophys. Res. Lett. 25, 1577–1580.

Yudin, P.V., Tagantsev, A.K., 2013. Fundamentals of flexoelectricity in solids. Nanotechnology 24, 43001.

Zubko, P., Catalan, G., Buckley, A., Welch, P.R.L., Scot, J.F., 2008. Strain gradient induced polarization in $StrO_3$ single crystals. Phys. Rev. Lett. 99, 167601.

Zubko, P., Catalan, G., Tagantsev, A.K., 2013. Flexoelectric effect in solids. Annu. Rev. Mater. Res. 43, 387–421.